Copyright Warning & Restrictions

The copyright law of the United States (Title 17, United States Code) governs the making of photocopies or other reproductions of copyrighted material.

Under certain conditions specified in the law, libraries and archives are authorized to furnish a photocopy or other reproduction. One of these specified conditions is that the photocopy or reproduction is not to be "used for any purpose other than private study, scholarship, or research." If a, user makes a request for, or later uses, a photocopy or reproduction for purposes in excess of "fair use" that user may be liable for copyright infringement,

This institution reserves the right to refuse to accept a copying order if, in its judgment, fulfillment of the order would involve violation of copyright law.

Please Note: The author retains the copyright while the New Jersey Institute of Technology reserves the right to distribute this thesis or dissertation

Printing note: If you do not wish to print this page, then select "Pages from: first page # to: last page #" on the print dialog screen

ABSTRACT

EFFECTS OF API PARTICLE SIZE ON THE DISSOLUTION RATE IN MOLTEN POLYMER EXCIPIENT MATRICES DURING HOT MELT EXTRUSION, CONDUCTED IN A CO-ROTATING TWIN-SCREW EXTRUDER

by
Meng Li

The effect of the Active Pharmaceutical Ingredient (API) particle size on the dissolution rate in the polymer excipient during hot melt extrusion is investigated using a co-rotating twin-screw extruder with three different screw configurations. Acetaminophen (APAP) and amphiphilic polyvinyl caprolactam-polyvinyl acetate-polyethylene glycol graft copolymer (PVCap-PVAc-PEG) (Soluplus®) are chosen as the model API and water-soluble polymer excipient, respectively. APAP is milled using a fluid energy mill (FEM) into two different particle sizes. The thermal properties of processed samples are characterized by TGA and DSC. SEM and optical microscopy are also used in the morphological studies. Under quiescent conditions, API particles with small particle size dissolve faster than the large ones. During the extrusion process using a co-rotating twin-screw extruder, fully-filled kneading blocks perform well in dissolving the API into the polymeric excipient matrices for both of APIs' particle sizes. However, screws with only conveying elements exhibit only limited ability in dispersing, distributing and melting APIs in the physical mixtures fed into the extruder, resulting in delayed and incompletely dissolution for all the API sizes.

EFFECTS OF API PARTICLE SIZE ON THE DISSOLUTION RATE IN MOLTEN POLYMER EXCIPIENT MATRICES DURING HOT MELT EXTRUSION, CONDUCTED IN A CO-ROTATING TWIN-SCREW EXTRUDER

by
Meng Li

A Thesis
Submitted to the Faculty of
New Jersey Institute of Technology
in Partial Fulfillment of the Requirements for the Degree of
Master of Science in Chemical Engineering

Otto H. York Department of
Chemical, Biological and Pharmaceutical Engineering

May 2013

APPROVAL PAGE

EFFECTS OF API PARTICLE SIZE ON THE DISSOLUTION RATE IN MOLTEN POLYMER EXCIPIENT MATRICES DURING HOT MELT EXTRUSION, CONDUCTED IN A CO-ROTATING TWIN-SCREW EXTRUDER

Meng Li

Dr. Costas G. Gogos, Dissertation Advisor — Date
Distinguished Research Professor of Chemical, Biological and Pharmaceutical Engineering, NJIT

Dr. Nicolas Ioannidis, Committee Member — Date
Research Engineer of Polymer Processing Institute

Dr. Ecevit A. Bilgili, Committee Member — Date
Assistant Professor of Chemical, Biological and Pharmaceutical Engineering, NJIT

Dr. Piero M. Armenante, Committee Member — Date
Distinguished Professor of Chemical, Biological and Pharmaceutical Engineering, NJIT

BIOGRAPHICAL SKETCH

Author: Meng Li

Degree: Master of Chemical Engineering

Date: May 2013

Undergraduate and Graduate Education:

- Master of Science in Chemical Engineering,
  New Jersey Institute of Technology, Newark, NJ, USA, 2013

- Bachelor of Science in Polymer Materials and Engineering,
  Shanghai University, Shanghai, P. R. China, 2011

Major: Chemical Engineering

I dedicate this to my beloved family.

ACKNOWLEDGMENT

I am extremely grateful to Prof. Costas G. Gogos, who not only served as my advisor, providing valuable resources, wise and strong academic guidance, but also gave me constant moral support and encouragement when I met with problems through my Master study. I feel highly honored that I obtained advice from this esteemed and knowledgeable advisor.

I also appreciate the involvement of Dr. Nicolas Ioannidis for his numerous instructive suggestions and active discussions with me throughout my work. Special thanks are given to Prof. Ecevit A. Bilgili and Prof. Piero M. Armenante for their participation in my thesis committee.

I wish to acknowledge the financial support received during my Master studies from research funds of Dr. Gogos. I also want to express my thanks to Polymer Processing Institute (PPI) for making their facilities totally available to me and for the advice I received from the technical staff. Also, I want to thank Ms. Mariann Pappagallo for helping me out with administration matters.

Finally, I give my deepest gratitude to my parents, Qinghai Li and Li Zhang and my younger brother, He Li. Their support, understanding, love, patience and sacrifice made me what I am now.

TABLE OF CONTENTS

TABLE OF CONTENTS
(Continued)

TABLE OF CONTENTS
(Continued)

Chapter **Page**

LIST OF TABLES

LIST OF FIGURES

LIST OF FIGURES
(Continued)

Figure **Page**

LIST OF FIGURES
(Continued)

Figure **Page**

LIST OF FIGURES
(Continued)

Figure **Page**

CHAPTER 1

INTRODUCTION

1.1 Objective

The dissolution rates of active pharmaceutical ingredient (API) in molten polymer excipient matrices during hot melt extrusion (HME) may be affected by the equipment, process and material parameters. The objective of this work is to study the effects of the API particle sizes, one of the material parameters, on their dissolution rates in the molten polymer excipient matrices during HME. This research was conducted in a co-rotating twin-screw extruder with three different screw configurations: two with kneading blocks at the 20^{th} (KS20) and the 8^{th} (KS08) lobes, and one with only screw conveying elements (CS). Additionally, an investigation was also conducted under quiescent conditions, using the hot stage microscope and DSC in ramp mode.

1.2 Background

Pharmaceutical hot melt extrusion (HME) is currently pursued actively by industry and academia to render poorly water-soluble active pharmaceutical ingredients (APIs) soluble in water-soluble polymers, enabling them to be bio-available. It involves the use of twin or single rotor extruders for the melting of water-soluble polymer excipients, mixing them with APIs and pumping the homogeneous mixture through a die to form an extrudate. The objective is to promote the partial or complete dissolution of the water-insoluble crystalline APIs into the molten water-soluble polymer excipient matrices, and make sure that the extruded HME product stays completely dissolved in the excipients for the expected shelf life of the oral dosage. Degradation of the drug (API)

and excipient may occurring during HME because of the relatively high processing temperatures and heating due to viscous energy dissipation (VED) and re-crystallization of APIs after the temperature drops from the elevated processing temperature to room temperature are the main areas of concern during HME.

The particle size is a significant parameter for a wide range of pharmaceutical preparations, since it influences dissolution, solubility or bioavailablility, processability, stability, dose-content uniformity, and appearance of drugs. A modified version of Noyes-Whitney equation (Noyes and Whitney 1897) (Equation 1.1):

$$\frac{dW}{dt} = k_0 A(C_S - C) \tag{1.1}$$

can be used to describe the API dissolution rate. Here, k_0 is the overall solute transfer coefficient defined by $1/k_0 = 1/k_i + 1/k_c$, where k_i and k_c are the interface rearrangement constant and the external mass transfer coefficient, respectively, C_s is the saturation solubility, C is the concentration in the bulk solution, A is the total surface area, and W is the amount dissolved at time t.

The increase in dissolution rate of particles can be explained by three effects, according to the above equation. During HME, the major contribution to the enhanced dissolution rate of the drug is through the specific surface area and the total area A of the drug particles, both of which increase due to size reduction. As the particle size of the APIs is reduced, the total surface area of the drug particles exposed to the polymeric melt is increased, the interface between the drug and polymer particles become larger,

increasing the effect of particle-to-particle friction and diffusion, thus enhancing the dissolution rate.

APIs with smaller particle sizes can be produced by size reduction of larger particles. (Teng et al. 2009) (Wang et al. 2009)

The dissolution of API in the polymer melt during HME is a laminar forced convective diffusion process. Both dispersive and distributive-mixing processes inside the extruder may significantly enhance the dissolution rate. When micronized drugs are mixed with excipients prior to processing into dosage forms, a complex array of particulate forms can exist due to cohesive and adhesive particle interactions present within the mixture. These particulate forms include interactive units and agglomerates of varying compositions (Supabphol and Stewart 1996). Both distributive as well as dispersive mixing are needed to dissolve the API homogeneously. It should be mentioned that, in the drug and polymer systems, dispersive mixing may break up the drug agglomerates or even individual particles due to the high shear forces generated by the high shear screw elements such as wide kneading blocks (Tadmor and Gogos 2006). Under dynamic conditions the melting is mainly due to the plastic energy dissipation (PED) and frictional energy dissipation (FED), and dissolution to the mainly extensional flows, both induced in fully-filled kneading elements. Under quiescent conditions, such as DSC ramp heating of physical mixtures and hot stage microscopy, the melting and dissolution of the physical mixture are only affected by the conduction heating.

CHAPTER 2

LITERATURE REVIEW

2.1 Pharmaceutical Hot-melt Extrusion (HME)

Pharmaceutical Hot Melt Extrusion (HME) is a term that the pharmaceutical sector adopted to differentiate it from traditional oral dosage producing techniques, such as direct compression and tableting. Because of its potential of rendering poorly water-soluble active pharmaceutical ingredients (APIs) readily bioavailable to patients through oral dosages, pharmaceutical HME has been explored and studied in the last two or so decades by both industrial and academic investigators. This field is currently investigated even more intensively, due to the recent discoveries of large families of potent and promising, but essentially water-insoluble APIs.

Compared to the traditional drug production processes, HME is a solvent-free continuous process, and it may lead to fewer required processing steps. It is generally accepted that polymer compounding involves five elementary steps: handling of particulate solids, melting, mixing, devolatilization and stripping, pressurization and pumping (Tadmor and Gogos 2006). In pharmaceutical HME, the additive compound is an API, which can dissolve in the molten excipient. Thus, total or partial dissolution of the API into the excipient matrices becomes the sixth elementary step, taking place after exipient melting and aided by efficient laminar flows generated by fully-filled kneading elements.

Pharmaceutical HME is generally divided into two categories, depending on the processing temperature. The most common case (Case I) is that where the processing temperature is above the melting temperature of semi-crystalline polymers or (50-100) °C

above the glass transition temperature T_g of amorphous polymers, but below the melting temperature of the crystalline API. Another case (Case II) is one where the processing temperature is above the melting or glass transition temperature of polymer excipient and above the melting point of the API (Gogos et al. 2012). Case I is preferable, because it presents less of a threat to thermal degradation of the API. Typically, the processing temperature refers to the melt temperature rather than the twin- screw extruder barrel setting temperature.

It is to be noted from the above comments that, due to degradation of the drug (API) and excipient during HME at the relatively high processing temperatures needed to melt the excipient and the laminar flow viscous energy dissipation heating, there is no 'universal' application of HME for all API/excipient pairs.

2.1.1 Elementary Steps in HME

HME involves six elementary steps as mentioned above: handling of particulate solids, melting, mixing, dissolution, devolatilization/stripping, as well as pressurization/pumping (Tadmor and Gogos 2006). The two most important elementary steps for plastics compounding are melting and dispersive and distributive mixing of the additives in the polymer matrices, while, for pharmaceutical HME processing, dissolution of the API in the molten excipient is an additional and equally important elementary step, along with melting and mixing. As mentioned above, melting of polymer excipients precedes the dissolution of the API in the molten excipient and efficient laminar mixing assists and speeds up dissolution.

The features of the elementary steps relevant to HME process and products are briefly reviewed (Liu 2010):

Particulate Solids Handling (PSH): Single screw extruders (SSE) are 'flood fed' through hoppers, the feed being a mixture of the excipient and API in particulate form. In co-rotating twin-screw extruders (Co-TSEs), which are commonly used in HME process development, the PS ingredients are fed gravimetrically or volumetrically, controlled at constant rates smaller than those needed to fully fill the parallel channels, resulting in 'starve-fed' processing. This PSH in Co-TSEs may result in spatial particle segregation when the relative sizes or shapes of the API and the Excipient are very different. Their difference in flowability results in different air resistive forces and different particle/wall kinematic friction coefficient.

Melting: In SSEs, melting is localized at the barrel surface and is gradual, requiring much of the extruder length to complete. The conductive melting of the packed particulate bed surface next to the hot barrel surface, and, after the thickness of the melted polymer layer exceeds that of the barrel-screw tip clearance, also viscous energy dissipation during the drag flow will cause the removal of the melt generated to the trailing end of the bed. The melting in a typical SSE results in a wide 'age-distribution' of the order of the residence time. In Co-TSEs, the available melting mechanisms of conductive melting by the hot barrel are significant for the small Co-TSEs, where the surface-to-volume ratio is large. However, for larger diameter Co-TSEs, reverse screws or reverse kneading elements are used to create a filled section, in which the packed particulates undergo repeated volume-wide deformations of the order of one strain unit before exiting the fully filled region. In the fully-filled region, the powerful melting mechanisms are plastic energy dissipation (PED) as well as the particulate-to-particulate

frictional heating and localized melting because of frictional energy dissipation (FED) (Tadmor and Gogos 2006) (Gogos et al. 1998).

Devolatilization: This step refers to the removal of low levels of volatiles dissolved in the molten matrices, which is carried out in vented two-stage SSEs and Co-TSEs in partially filled sections isolated from both the upstream and downstream sections by 'melt seals', which consist of fully-melt-filled axial regions of the extruder. The dissolved molecules form bubbles under vacuum conditions in the flowing melt stream, burst in the melt-vacuum interface, and are removed (Tadmor and Gogos 2006).

Pumping and Pressurization: Pumping the molten charge through a die is an essential step for extruders, after they accomplish all the other elementary steps, to shape the exiting stream in operations such as pelletization, and sheet, film, tube, or profiled cross-section products. Drag-induced pumping and pressurization enable both SSEs and Co-TSEs to be the pumps of choice for viscous fluids. SSEs can generate higher pressures under closed discharged conditions, because their flight heights can be small in the pumping section upstream the die. On the other hand, Co-TSEs are incapable of generating high pumping pressures, which limits in cases of very viscous extrudates. The reason is that Co-TSEs are fully intermeshing and self-wiping, which is advantageous for HME operations, because they eliminate "dead" molten polymer regions, which would result in thermal degradation. Chill rolls and/or cold air are generally used in cooling strand extrudates, but not water-cooling, since excipients are water-soluble.

2.1.2 Dispersive and Distributive Mixing

Laminar dispersive and distributive mixing of API particulates in the molten excipient occurs simultaneously with the desired dissolution of the API. They are two types of mixing mechanisms in single- and twin- screw extruders.

Dispersive mixing refers to the process involving the particle size reduction of cohesive minor components such as solid fillers by de-agglomeration, or liquid droplets by droplet deformation and breakup. The balance between the cohesive forces holding agglomerates or droplets together and the disruptive/dispersive hydrodynamic forces determines the conditions under which dispersive mixing occurs. The occurrence of dispersive mixing requires high flow stresses, either through high viscosity of high shear or elongational rates, in order to provide the dispersive forces to overcome the cohesive forces of the agglomerates or immiscible droplets (Liu 2010). Distributive mixing refers to distributing de-agglomerated particulates uniformly throughout space or stretching the interfacial area between the components lacking a cohesive resistance and distributing them uniformly throughout the processed stream volume in order to obtain a good spatial distribution. However, in contrast to dispersive mixing, distributive mixing is dictated only by the flow-generated strain and does not require high stresses.

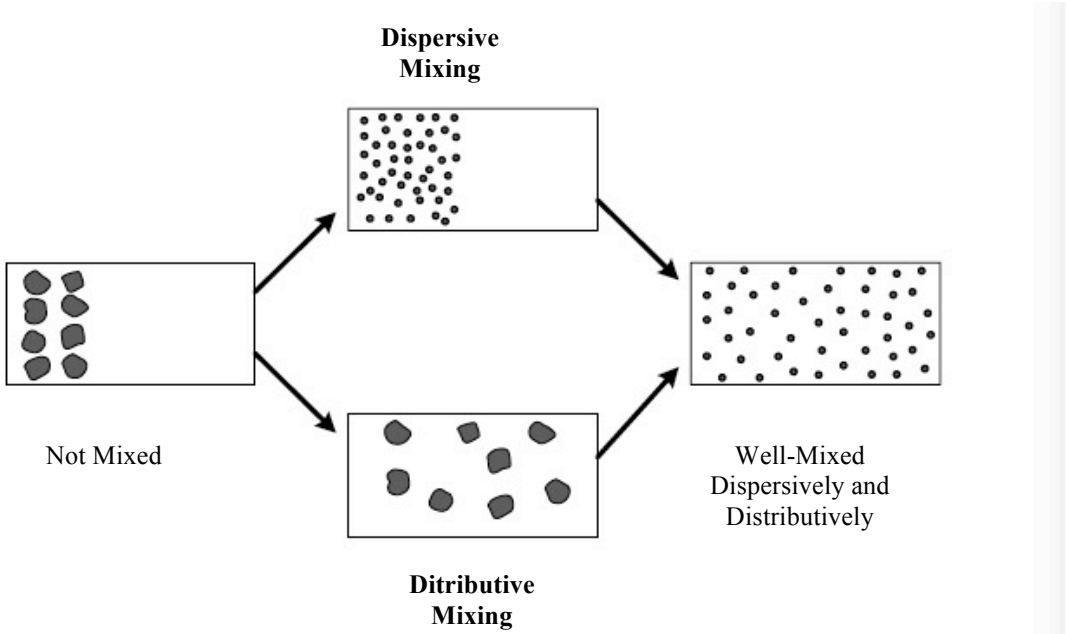

Figure 2.1 Schematic representation of dispersive and distributive mixing of solid agglomerates and immiscible liquid droplets. (Tadmor and Gogos 2006)

Both dispersive and distributive mixings play key roles on the dissolution of the drug into the polymeric excipient melt. However, in the system, where the drug particles do not form agglomerates, there is no evidence that dispersive mixing is involved because the size reduction of drug particles is due to the diffusion of the drug molecules to the polymeric melt rather than shear forces (Liu et al. 2010). But in other systems, dispersive mixing may break up the drug agglomerations or even particulates by the high laminar flow forces induced by either material properties like excipient viscosity, operating variables like screw speed or extruder design variables like the screw configurations in co-TSEs.

2.1.3 Melting and Dissolution in Extrusion

Melting precedes the dissolution of the API in the molten excipient and assists and speed up dissolution. For pharmaceutical HME processing, dissolution of the API in the molten excipient is an additional and most important elementary step, along with melting and mixing.

The physical mechanisms that can bring about melting or heating of any substance are included in the terms of the thermal energy balance. (Tadmor and Gogos 2006)

$$\rho \frac{Du}{Dt} = -\nabla \bullet q - P(\nabla \bullet v) - (\tau : \nabla v) + \dot{S} \tag{2.1}$$

The internal energy of a material can be raised by four sources, each one of which represents heating mechanisms, as indicated in the equation. $(-\nabla \bullet q)$ presents the net rate of internal energy increase per unit volume from an outside source by heat conduction; $[-P(\nabla \bullet v)]$ presents the (reversible) rate of internal energy increase per unit volume by compression; $[-(\tau : \nabla v)]$ presents the (irreversible) rate of internal energy increase by flow and deformation; and $\dot{S}$ presents an additional possible homogeneous energy source.

Melting of polymers is generally classified into conduction melting, compressive melting, deformation melting and homogeneous internal melting. Conduction melting is the most common mode, which raises the temperature of a solid and melts it. As the surface temperature of the solid is raised, a molten layer is formed and it grows with time. Thermal conductivity, attainable temperature gradients, and available contact area between the heating source and the melting solid are the rate-controlling factors of

conduction melting.

For polymers, which have low thermal conductivity and high temperature sensitivity, the conduction melting is inefficient. However, in flood-fed single screw extruders, drag-induced melt removal takes place. The SSE quickly removes the freshly molten material from the vicinity of the high temperature zone, which reduces the risk of degradation. Also, it generates heat via viscous energy dissipation, which increases the efficiency of melting.

Deformation melting of polymer solids involves irreversible conversion of mechanical energy to heat. Deformation heating, in flowing viscous liquids, especially when the shear rates under processing conditions are high is also significant. In the melting step of polymer processing, repeated deformation is imposed on a compacted bed of particulate solids, which generates significant, but non-homogeneous heat energy, called plastic energy dissipation (PED) and frictional energy dissipation (FED) for individual polymeric particles undergoing repeated deformations and generating heat within the particle and the mechanical energy dissipated into heat via inter-particle friction, respectively. PED and FED play predominant role in processing equipment, in particular in co-rotating twin screw extruders (Co-TSEs). In this case, the thermal energy equation can be written as (Tadmor and Gogos 2006):

$$\rho_S C_S \frac{DT}{Dt} = -\nabla \bullet q + PED + FED \tag{2.2}$$

Since the fact that polymer solids and melts are virtually incompressible and other homogeneous internal melting, like dielectric heating, are limited in polymer processing

practice, according to criteria of avoiding thermal degradation and achieving high processing rates, the melting mechanisms for polymers are summarized as: conduction melting with forced melt removal (by SSE), plastic energy dissipation (PED) and frictional energy dissipation (FED) (by twin rotor devices), and dissipative mix-melting (DMM) (by twin rotor co- and counter- rotating devices) (Tadmor and Gogos 2006).

Co-rotating twin screws with only conveying elements act similarly to single screw, which convey and compress the physical mixture by a drag-induced mechanism, then melt by a drag-induced melt removal mechanism. However, because of their unique time-varying screw-to-screw interactions taking place, additional physical mechanisms emerge, which may primarily affect the elementary step of melting and mixing. In other configurations of TSEs, due to the addition mechanisms, melting and mixing steps are carried out more efficiently and uniformly, thus narrowing the residence time distribution (RTD) in the molten state. In SSEs, on the other hand, some of the polymer melts early in the extruder and some at the very end, and hence, the RTD in the molten state is rather broad.

Melting in Co-TSEs in fully-filled kneading blocks takes place primarily and most commonly in the kneading elements where particulates are fully compacted because of a flow restriction. The evolution of melting in such filled kneading-elementary channels was studied experimentally by Kim (Kim 1999) and Gogos et al. (Gogos et al. 1998). They found that inter-particles FED takes place early and does not require full compaction, but does require particle-to-particle sliding and normal forces. At full compaction, PED becomes the dominant melting mechanism.

The dissolution of APIs into the polymeric excipient may largely depend on their

physicochemical properties. Good miscibility between APIs and polymer excipients is the key requirement for solid dispersions to increase physical stability (Marsac et al. 2008). In practice, the majority of drug/polymer systems are likely to show only partial miscibility (Craig 2002), which means that there exists a certain thermodynamic solubility of drugs in polymer matrices. The solubility parameter is a measure of cohesive energy density (CED: the cohesive energy per unit volume) of the materials. The difference between the drug/excipient solubility parameters is widely used to predict their miscibility. Namely, if the difference is <7.0 $MPa^{1/2}$, the two components are likely to be miscible and form a solid glassy solution; if >10 $MPa^{1/2}$, they are likely to be immiscible, and formation of a solid glassy solution is unlikely. (Greenhalgh et al. 1999) (Forster et al. 2001) (Chokshi et al. 2005)

HME processes are generally classified into two categories (Gogos et al. 2012):

Case I: in which the processing temperature is above the melting temperature (semi-crystalline polymer) or (50-100) °C the glass transition temperature of an amorphous polymer, T_g, but below the melting point of a crystalline API.

Case II: in which the processing temperature is above both the melting or softening temperature of semi-crystalline or amorphous polymers, respectively, and above the melting point of the API.

Case I provides a viable dissolution path which minimizes or circumvents the thermal degradation issue of drugs resulting in a desirable polymer-drug solid dispersion or solid solution, in which the solid API acts as a solute dispersion and the polymer excipient melt acts as a highly viscous solvent. On the other hand, it is expected that the

dissolution rates and the solubility are larger in the case that the processing temperature is higher. Figure 2.2 shows its physical model schematically.

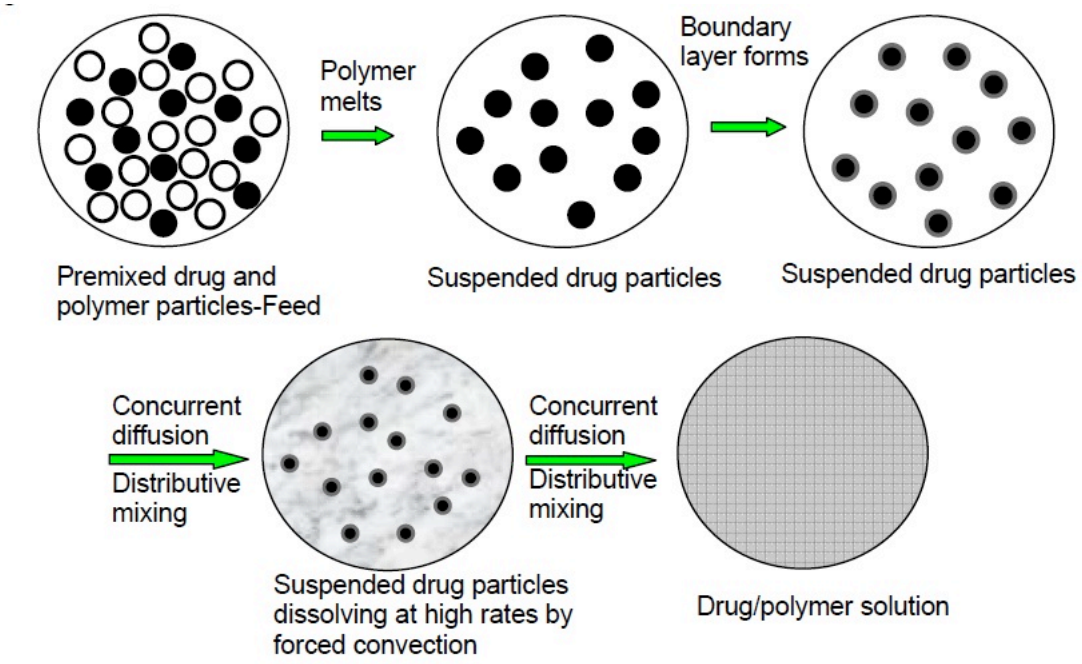

Figure 2.2 Schematic representation of the morphological changes of the drug and polymer system in the solution formation process (Case I). (Gogos et al. 2012)

The premixed drug (black) and polymer particles (white) are fed into a batch mixer or an extruder. The polymer particles start melting due to the conductive heat from the mixer or extruder barrel and frictional and plastic energy dissipation for co-TSEs, leading to the solid drug particles being suspended in a continuous polymer melt matrices. While suspended at the processing temperature, which favors dissolution assuming intermolecular forces compatibility between the API and the excipient, the drug molecules start dissolving and create a mass-transfer boundary layer around each drug particles. This layer is continuously wiped away and replaced by fresh polymer melt around each API particulate by the laminar distributive flow of the mixer. The same laminar mixing flow helps the drug molecules to diffuse and mix distributively into the

molten excipient. The size of suspended drug particles diminishes as the diffusion continues until the particles disappear and a homogeneous solution formed or until the limit of API solubility at the processing temperature is reached. In the latter case, they reach a minimum average size and remain suspended. The dissolution of the drug in the polymer melt in an extruder is achieved by laminar forced convective mass transfer involving the dissolving and dissolved API molecules.

The main and delicate task of Case I is to completely dissolve API in the polymeric melt within the shortest possible residence time without raising the processed stream melt temperature.

Case II involves liquid-liquid mixing between of miscible or partially miscible components. The morphology changes are shown in Figure 2.3.

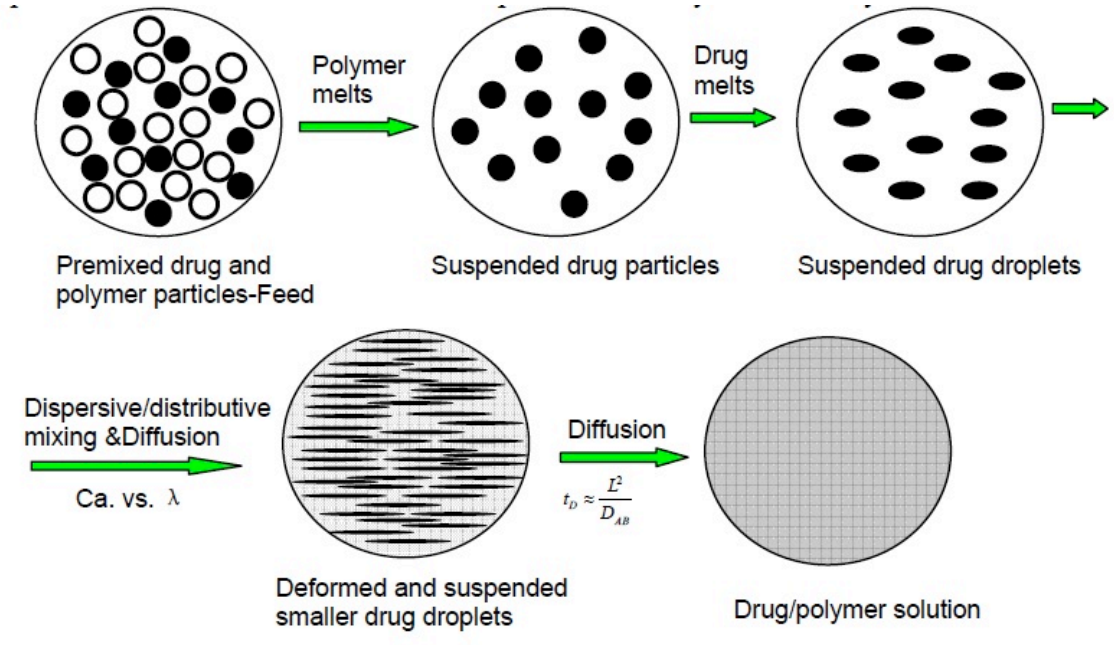

Figure 2.3 Morphological changes in drug/polymer system for Case II. (Gogos et al. 2012)

The premixed drug (black) and polymer (white) particles are fed into an extruder and conveyed by the conveying elements. The polymer particles melt first due to the energy input from the barrel and frictional and plastic dissipation. After the polymer particles totally or partially melt, the drug particles suspended in the molten polymer melt rapidly, and the drug droplets begin to be deformed by the mixing laminar flows of the polymer melt rapidly, and the drug droplets begin to be deformed by the mixing laminar flows of the polymer melt. After that, the drug liquid phase breaks up into much smaller droplets due to the competition of surface tension and flow stress. The small droplets are deformed along the shear direction. With numerous very small droplets, which have an enormous surface, diffusion between the droplets and the polymer predominates causing the droplets to disappear, creating drug-polymer solution.

Diffusion occurs in both cases during the dissolving of API particles in the molten polymer matrices and the break-up of the large drug droplets. Note that the 'characteristic diffusion time' t_D is proportional to the square of the API phase droplet or ligament radius or the thin dimension of a sheet (Equation 2.3).

$$t_D \approx \frac{L^2}{D_{AB}} \tag{2.3}$$

Similarly to the dissolution of drugs in an aqueous medium, the dissolution of drug particulates in molten polymer excipients, during HME, can also be described by the Noyes-Whitney equation given in Equation 1.1, which can be modified as follows:

$$\frac{dC}{dt} = \frac{D \times A \times (C_s - C)}{h \times V} \tag{2.4}$$

where D is the diffusion coefficient of drug; A is the total surface area of the drug exposed to the dissolution media; C_s is the saturation solubility of the drug in the liquid which (for HME) is the excipient melt; C describes the concentration of the dissolved solid phase in the bulk at time t; h represents the diffusion boundary layer at the solid-liquid interface; and V is the volume of the dissolution medium.

In both the diffusion and dissolution cases, the particle sizes of API in the molten excipient-API system play a significant role. The diffusion rate as well as the dissolution rate of drug particulates in polymer melt will increase if the total surface area of the drug particulates exposed to the dissolution media increase. Furthermore, the narrower the drug particle size distribution, the more uniform the total dissolution time distribution needed for complete dissolution of drugs in polymer melt will be. (Gogos et al. 2012)

2.2 Characterization Methods

The objective of processing a pharmaceutical formulation using HME is to dissolve all or part of the APIs into the polymeric excipient matrices and keep them in their amorphous form during the cooling of the HME extrudate. Also, investigations are conducted on their dissolution process inside the extruder; in which case, sample extrudates are taken along the screws. To characterize the physical nature of extrudates at molecular or microscopic level, several methods can be used.

2.2.1 Thermo-analytical Methods

The thermal properties can affect the dissolution, bioavailability and stability of the HME product performance. Besides, the thermal stability of the individual component indicated by the Differential Scanning Calorimetry (DSC) and/or thermogravimetric analysis (TGA) is essential for the process conditions during HME.

DSC is the most common application for thermal analysis. It is generally accepted that the absence of endothermic melting peak of the crystalline drug indicates that the drug is present in an amorphous rather than crystalline form. The crystal detection limitation of DSC is about 2 % (Leuner and Dressman 2000). The DSC device maintains the same programmed heating rate in each heater and records the power required to achieve this. If a transition takes place in the sample, a characteristic excursion in the measured differential power is observed (Thompson 1985).

For some cases, there may not exist a drug-melting peak during DSC scanning even for a physical mixture. For example, Lloyd et al. reported that the physical mixture of 20 % acetaminophen/polyethylene glycol (PEG)-4000 formulations does not show a drug-melting peak (Lloyd et al. 1997a). In addition, the very broad endothermic peak which may appear on the first DSC scanning may be related to the dissolution of remaining crystalline drug particulates (Qi et al. 2008).

Hot stage microscopy (HSM) allows visual observation of the thermal events of sample formulations through a microscope during heating and cooling cycles. Lloyd et al. found that HSM is far more sensitive to the presence of small quantities of solid drug than DSC (Lloyd et al. 1997b) when studied the preparation of a solid dispersion of acetaminophen and polyethylene glycol (PEG) 4000.

2.2.2 Microscopic Methods

Optical and electron microscopes can help determine the existence of drug crystal regions and their size as well. Although the resolution of polarized light microscopy (PLM) is approximately at 1 μm, the birefringence of the crystal drug imparts a sharp and distinct contrast against the amorphous (dark) excipient. Yoo et al. studied the miscibility/stability for 24 binary solid dispersion systems and found that the sensitivity to crystal detection was PLM > DSC > XRD (S.U. Yoo 2009). Bruce et al. employed SEM for in-situ observation of crystal growth in melt extrudates (Bruce et al. 2007).

SEM makes use of a beam-scanning mode of operation. A fine electron beam scans the surface of the specimen previously coated with a conducting layer in a two-dimensional raster. The back scattered or the secondary electrons are analyzed with a scintillation counter, and the signal from the counter is fed into a cathode-ray tube, which is set to scan synchronously with the electron beam. As a result, a point-by-point image of the specimen is displayed on the cathode-ray tube. In order to increase the electric conductivity of the tantalum layer, a subsequent carbon layer has to be deposited by flash evaporation of carbon yarn (Doll et al. 1985).

CHAPTER 3

MATERIALS AND METHODS

3.1 Materials

The crystalline Acetaminophen (APAP) with a melting temperature around 173 °C was chosen as the model drug. Soluplus (PVCap-PVAc-PEG) was used as the model polymeric excipient. This polymer is an amphiphilic polyvinyl caprolactam-polyvinyl acetate-polyethylene glycol graft copolymer and is amorphous with a single glass transition temperature (T_g) of 73 °C ± 2 °C. The difference in solubility parameter between APAP and Soluplus is 6.78 MP^{-1}. According to the criterion accepted in literature (Greenhalgh et al. 1999) (Forster et al. 2001), APAP and Soluplus are likely to be miscible. The API/Polymer weight ratio of the system used was kept at 30: 70 throughout this study. The bulk densities of the APAP, the Soluplus and the physical mixture of APAP and Soluplus (30/70) are 0.33, 0.52 and 0.61 g/cm^3, respectively. All raw materials were in powder form. The angles of repose of APAP and Soluplus are around 70 ° and 10 °, respectively.

3.2 Reduction of Particles Size

An FEM qualification unit (diameter: 2 inches) manufactured by Sturtevant, Inc. (Hanover, MA) was used in this work to reduce the mean particle size of APAP. The FEM unit includes three air inlets: two grinding air inlets and one feed air inlet. The feeding pressure and grinding pressure were set 55 MPa and 40 MPa, respectively. The solid particles are fed into the feed funnel and then sucked into the chamber through the Venturi region by the feed air. The milled particles escape the chamber from an exit tube

located in the center of the top plate of the FEM chamber. The particle sizes were determined by the SEM images. Samples of two different particle sizes were labeled as original, milled API - APAP 1# and APAP 2#.

Physical mixtures (PM) of API/Polymer (30/70 weight percentage) were prepared using a rolling blender at 250 rpm for 25 min.

PM 1#: original APAP/Soluplus.

PM 2#: milled APAP/Soluplus.

Table 3.1 Table of APAP Particle Sizes in Different Physical Mixtures

Physical Mixtures of APAP/Soluplus	**PM 1#**	**PM 2#**
Particle Sizes of APAP in the PM (μm)	100-200	5-10

3.3 Extrusion

The APV MP2015 (APV UK) was used to investigate the evolution of the morphology of materials along the screws and the effect of cohesion on the dissolution of the API. The diameter of the APV MP2015 screws is 15 mm, and the ratio of the barrel length to the screw diameter is 15. The barrel consists of three heating zones, all at the same set temperatures. The feeding "throat" underneath and just upstream the feeder was cooled by tap water. The melting temperature sensor installed inside the die measured the actual process stream temperature. The PM was fed into the extruder by a volumetric feeder (SCHENCK AccuRate® 102M) using an average feeding rate of 3.6 g/min (0.22 kg/h).

To figure out the temperature for the full dissolution of drug particles into the polymer, the temperatures of barrel and the die were set at 95 °C, 100 °C, 110 °C and 120

°C using the KS20 screws. The screw speed employed throughout was 70 rpm. The original APAP/Soluplus (30/70) extrudates were labeled as Extrudate 1#95, Extrudate 1#100, Extrudate 1#110, Extrudate 1#120.

For the morphological evolution study, once the extrusion process reached a steady state, which is roughly determined by the residence time, the feeder and the extruder were stopped and the screws were rapidly pulled out. Samples were collected along the screws, cooled down using two pieces of metals to prevent the drug from further dissolving into polymer matrices, and labeled according to the number of lobes along the screws they were sampled from.

3.4 Batch Mixing

A Brabender FE-2000 counter-rotating batch mixer (C.W. Brabender Instruments Inc., South Hackensack, NJ) was used to mix original APAP particulates and Soluplus. This process is in the family of Hot Melt Mixing (HMM) operations, resulting in mixing similar to that generated in the axial design in the TSE. The mixer is equipped with temperature and torque meters to measure and record the actually melting materials' temperatures and the resistance to screws rotating caused by the presence of materials, respectively. The residence time can be controlled separately from other parameters since the device is a batch mixer. The barrel temperature was kept at 100 °C and the rotor screw speed was controlled at 50 rpm by a controller. The processing temperature was above the Soluplus' glass transition temperature, but lower than the melting temperature of APAP. Generally, about 70-75 vol.% fill degree of the chamber is recommended for good mixing because the resulting "folding" of the free surfaces is beneficial to

distributive mixing. The free volume in the mixing chamber is 60 cc. The bulk density of the physical mixture was roughly measured to be 0.61 g/ml. Thus, 27g of the physical mixture was used to achieve a 75 vol.% fill degree. The physical mixture was introduced into the batch mixer using a feeding chute. Samples were taken at 90 s, 270 s, 540 s. The weight of each of the samples was around 0.4 g. The samples were cooled by placing them between two pieces of metal and then characterized using different analytical characterization tools.

3.5 Compressing and Grinding

To simulate the dispersion effect, which may reduce the API particles size during HME conducted in co-rotating twin-screw extruder with intense kneading block, original APAP and their physical mixtures were compressed and ground using compressor and mortar and pestle.

A Carver Benchtop manual press, Model C (Wabash, IN) was used to make the tablets of APAP, Soluplus and their physical mixture (30/70). The samples weighed 1.0 g each. The pressure of the press was set around 14,000 psi. The diameters of the tablets of Soluplus and the PM are 2.6 cm. The one for the APAP tablet is with a diameter of 1.3 cm.

The raw material APAP and the physical mixture were ground using the mortar and pestle to investigate the APAP particle size changes.

3.6 Differential Scanning Calorimetry (DSC)

DSC of all samples was carried out using a TA Instrument Q100 (New Castle, DE) to get characteristic thermal transition temperatures, including the glass transition temperature

of Soluplus, the melting temperature of APAP. All extrudate samples were ground into fine powders using the mortar and pestle. Samples were placed in an aluminum pan and crimped with an aluminum lid.

A heat-cool-heat mode was used to obtain the glass and melting transition characteristics of raw materials, in which the first heating cycle serves to remove the previous thermal history from the sample, the cooling ramp imposes a known thermal history on the sample, and the second heating ramp allows the sample to be measured with that known thermal history. In heat-cool-heat mode, the heating rate was 20 °C/min from -20 to 200 °C under nitrogen flow (40 cm^3/min) and the cooling rate was 10 °C/min from 200 to -20°C. In the ramp mode, which contains all the thermal transitions of the sample, the heating rate was 20°C/min from -20 to 200 °C, again under nitrogen flow (40 cm^3/min). In the isothermal mode, the temperature was kept at 100 °C for 10 min. The DSC data were analyzed using the instrument-available Universal Analysis 2000 software.

3.7 Thermogravimetric Analysis (TGA)

A TA Instruments Q50 thermogravimetric analyzer (New Castle, DE) was used in this work. The ramp mode was used to determine the thermal stability of the materials. The raw materials were placed in an aluminum pan and heated from room temperature to 400 °C at a heating rate of 40 °C/min under airflow. Isothermal mode was used to determine the stability of the materials at the processing temperature. In isothermal heating tests, powders were quickly heated to 100 °C at a rate of 50 °C/min and held isothermally for 16 min.

3.8 Polarized Light Microscopy (PLM)

A Carl Zeiss microscope (Thornwood, NY) was used to observe the morphologies of the particles of raw materials, surfaces and cross-sections of the tablets made by the compressor and the extrudate discs.

A hot stage (Mettler FP90) was used in conjunction with a Carl Zeiss microscope (Thornwood, NY) to observe the morphology evolution of raw materials and extrudate samples. The heating rate was set 20 °C/min from 30 to 200 °C. Pictures were taken every 10 °C.

3.9 Scanning Electron Microscopy (SEM)

The morphologies of APAP with different particle sizes were measured using a scanning electron microscope (LEO Field Emission Gun 153 Digital SEM) operated at an accelerating voltage of 10 KeV. The samples were coated with a thin layer of carbon using a Bal-Tee Med 020 Sputter Coater in order to improve the electrical conductivity prior to imaging.

3.10 Angle of Repose (AOR)

The repose angle of original APAP was measured by a Hosokawa powder tester (PT-N) to characterize its flowability. The procedure used to measure AOR was the standard ASTM D6393-99 test procedure, and each datum point is an average of at least three measurements, as required.

CHAPTER 4

RESULTS AND DISCUSSION

4.1 Characterization of Raw Materials

The thermal properties and morphologies of the raw materials were characterized and are reported in this section. The characteristic thermal transition temperature of APAP and Soluplus are presented in Figures 4.1 and 4.2. DSC was used to get characteristic thermal transition temperatures, including the glass transition temperature of Soluplus and the melting temperature of APAP. In Figure 4.1, the first heating curve shows that the melting peak of APAP is at 172.65 °C, the cooling curve shows that the APAP gets recrystalized at cooling rate of 10 °C/min, and the second heating curve is almost the same as the first one, which has a peak at 172.38 °C. This figure implies that the APAP gets fully recrystalized during the cooling process at the cooling rate of 10 °C/min employed. In Figure 4.2, the second heating curve shows that the glass transition temperature of Soluplus is 72.74 °C.

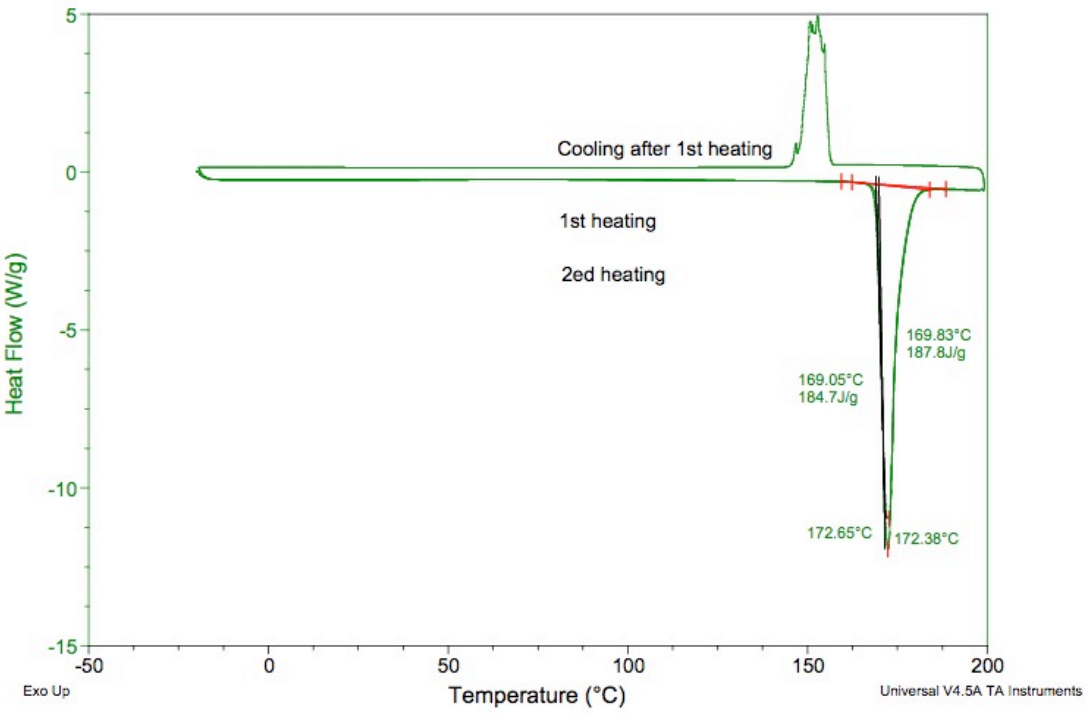

Figure 4.1 Conventional DSC results of APAP.

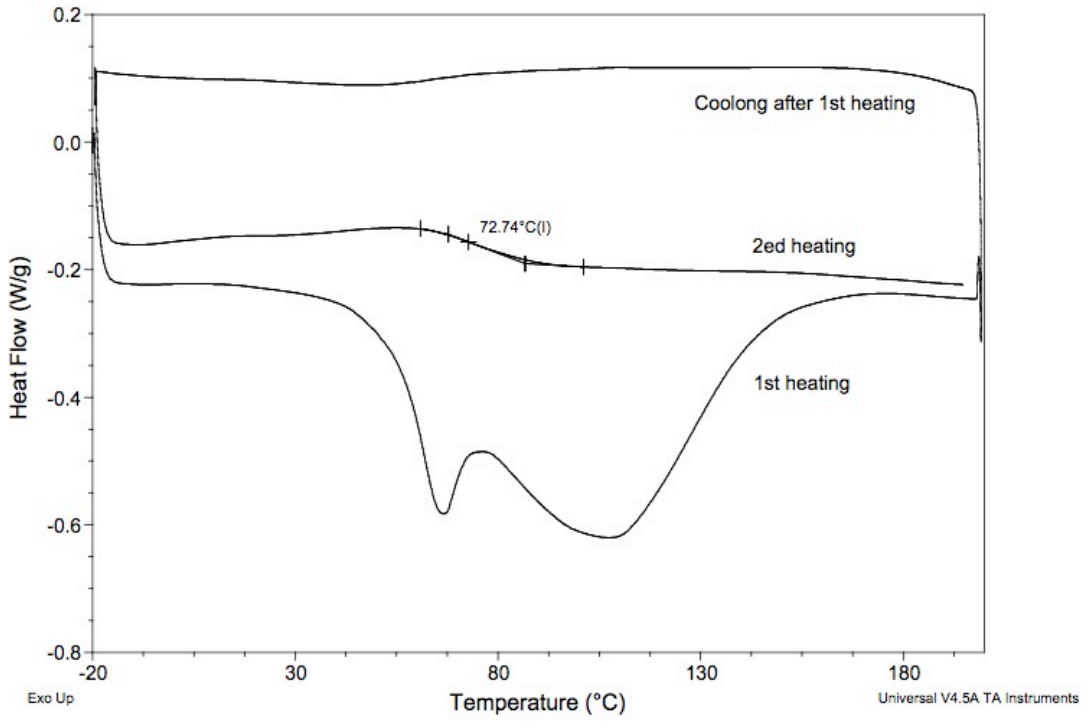

Figure 4.2 Conventional DSC results of Soluplus.

The TGA ramp results of APAP and Soluplus are presented in Figure 4.3. The onset temperature of weight loss in the TGA ramp heating tests is above 250 °C for 30 wt% APAP-Soluplus powder mixture, APAP and Soluplus. The 2 wt% weight lost by the polymer and PM starting at 75 °C corresponds to the loss of adsorbed water (Terife et al. 2012).

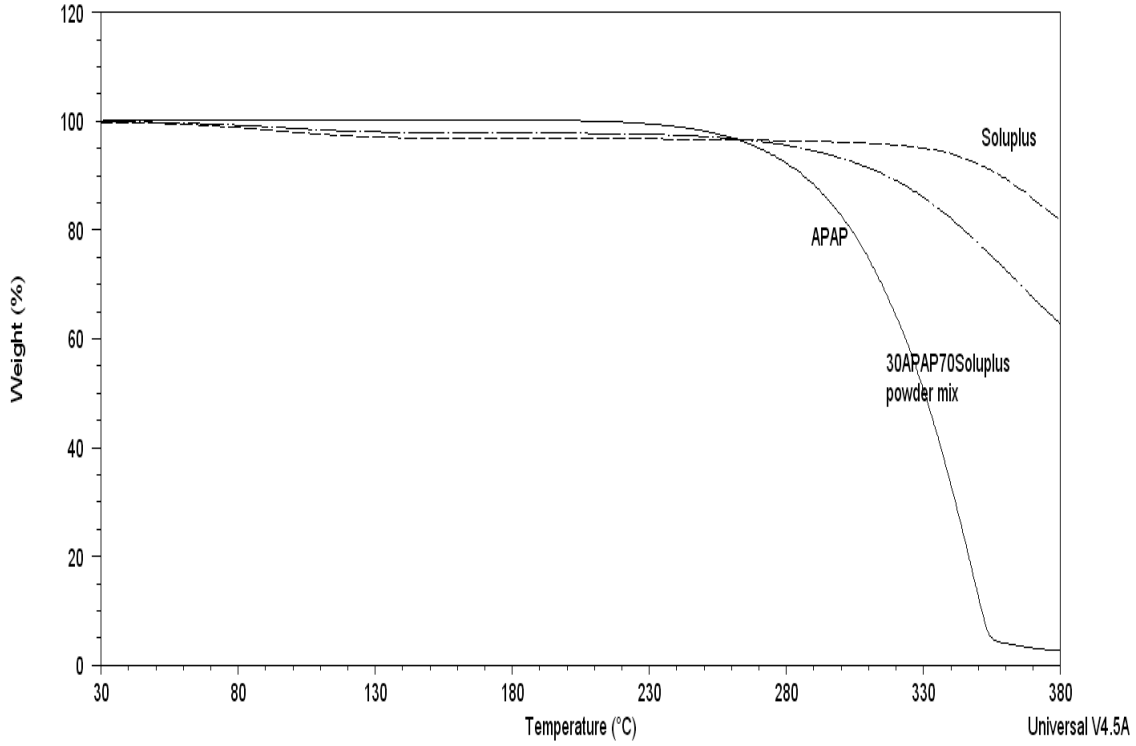

Figure 4.3 TGA ramp of APAP, Soluplus and 30 wt% APAP/Soluplus powder mixture heated in open air.

The isothermal TGA at the HME barrel temperature (100 °C) was conducted to further examine the thermal stability of PM, as shown in Figure 4.4. The isothermal test shows 2 % weight loss at 100 °C. The entire loss is recorded in the first 3 min, out of the total 16 min of the test in the air environment, and it is attributed to the absorbed water as

mentioned above. In these tests, all samples were processed for 10 min at 100 °C, a temperature which is far below the materials' degradation temperature.

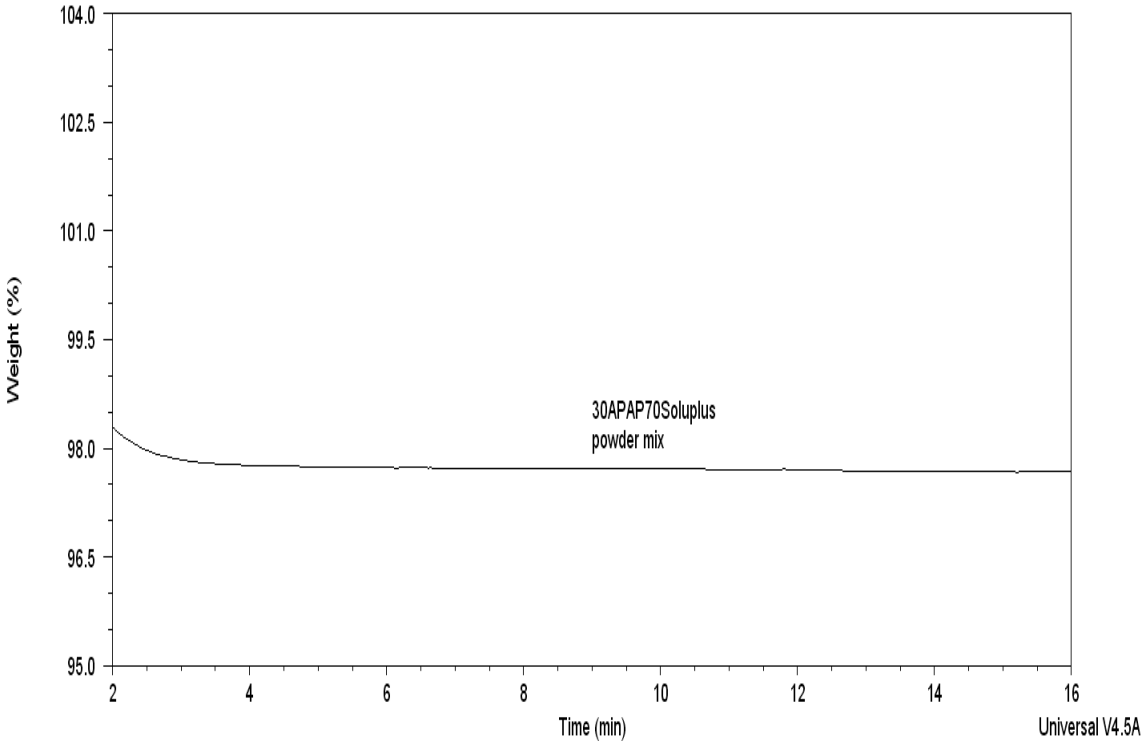

Figure 4.4 TGA isothermal heating of 30 wt% APAP/Soluplus powder mixture in 16 min in open air.

The morphologies were explored using an optical microscope and a scanning electron microscope (SEM). Figure 4.5 shows the optical microscope images of original and milled APAP particles.

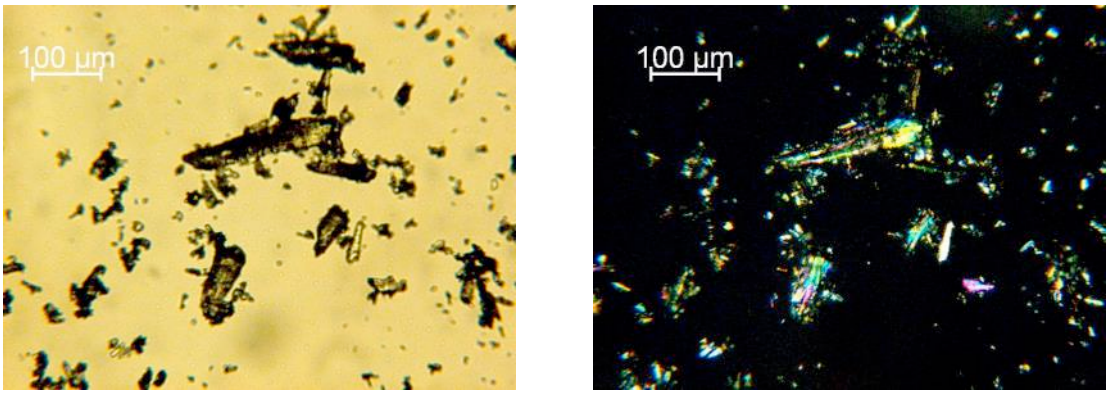

Original APAP Particles

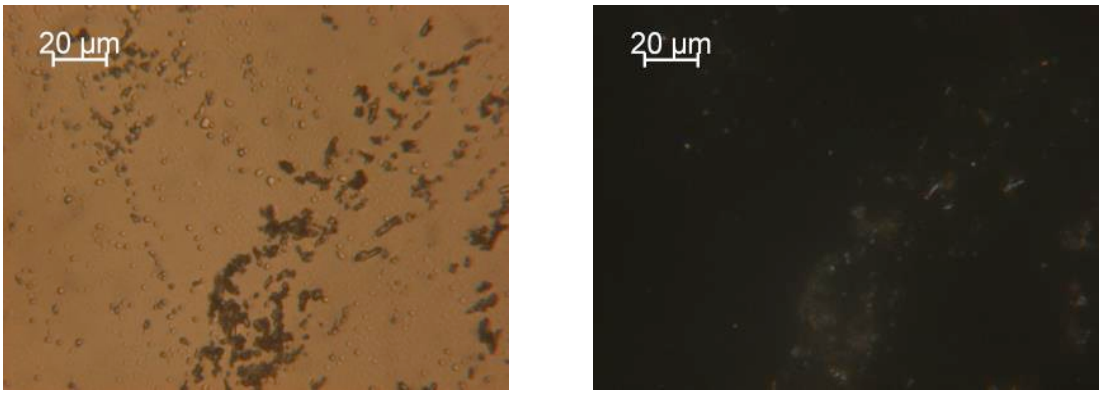

Milled APAP Particles

Figure 4.5 Transmission optical microscopy of original and milled APAP, without (left) and with (right) cross-polarizer.

The SEM images of the original and milled APAP are shown in Figure 4.6. The original APAP powders are needle-shaped crystals with the length 100-200 µm. Because the APAP particles are fragile (friable), they include a significant amount of fine powders. The milled APAP powders have particle sizes ranging from 5 to 10 µm. The intrinsic property of cohesion of the APAP particles renders the milled APAP into agglomerates.

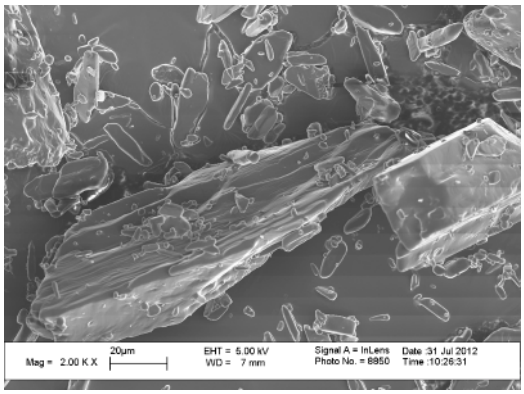

Original APAP Particles

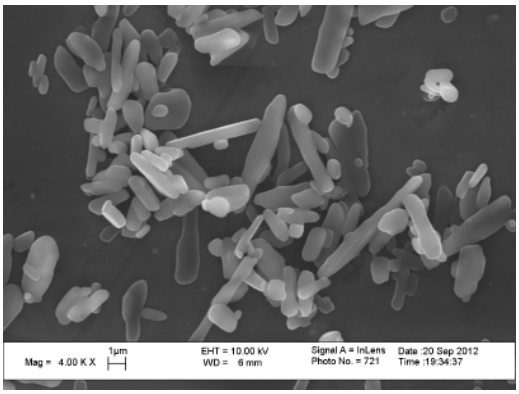

Milled APAP Particles

Figure 4.6 SEM morphologies of original and milled APAP particles.

The size of original APAP particles in Figure 4.6 is about 200 µm * 30 µm * 10 µm (length * width * thickness). The size of milled APAP is around 5 µm * 1 µm * 0.5 µm.

Figure 4.7 indicates that the original Soluplus has a particle size around 300 µm. The Soluplus particles are globular-shape and glandular at their surface, as seen from the optical microscope images.

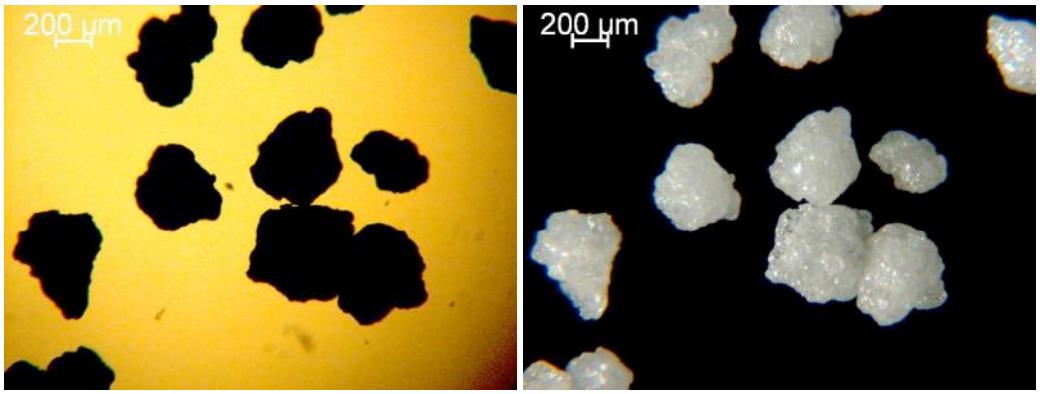

Figure 4.7 Transmission (left) and reflection (right) optical microscopy of Soluplus particles.

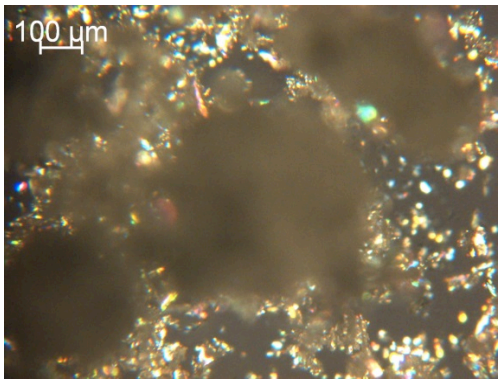

Original APAP/Soluplus

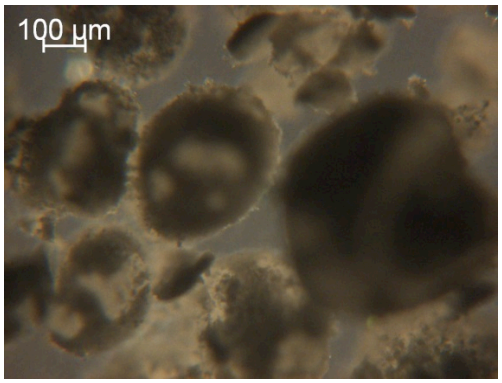

Milled APAP/Soluplus

Figure 4.8 Transmission optical microscopy of original APAP/Soluplus (30/70), milled APAP/Soluplus (30/70) physical mixtures, with cross-polarizer.

Figure 4.8 is the morphology of physical mixtures of original APAP/milled APAP and Soluplus (30 wt% API). In the figures, large globular-shape particulates are Soluplus

and the small needle-shape crystals are APAP. Because of large difference between particle sizes of the two components in the physical mixtures, the API particles are believed to coat and adhere to the surface of the Soluplus particles and, when exceeding surface saturation, API particles may attach to each other and form agglomerates.

Figure 4.9 Angle of repose of original APAP (left) and Soluplus (right).

The angle of repose of APAP is around 70 °, which is mainly due to its needle shape. Such a high AOR indicates very poor flowability, since the APAP particultes can support higher yield stresses. Soluplus, on the other hand, has a granular shape, resulting in an AOR of 10 °. However, the milled APAP are more cohesive and blocked the filling funnel, as shown in Figure 4.10. For this reason, the angle of repose of milled APAP was not measured, because there is practically no flowability. In order to become flowable they have to be mixed in dry-blend form with larger more flowable particulates, such as Soluplus.

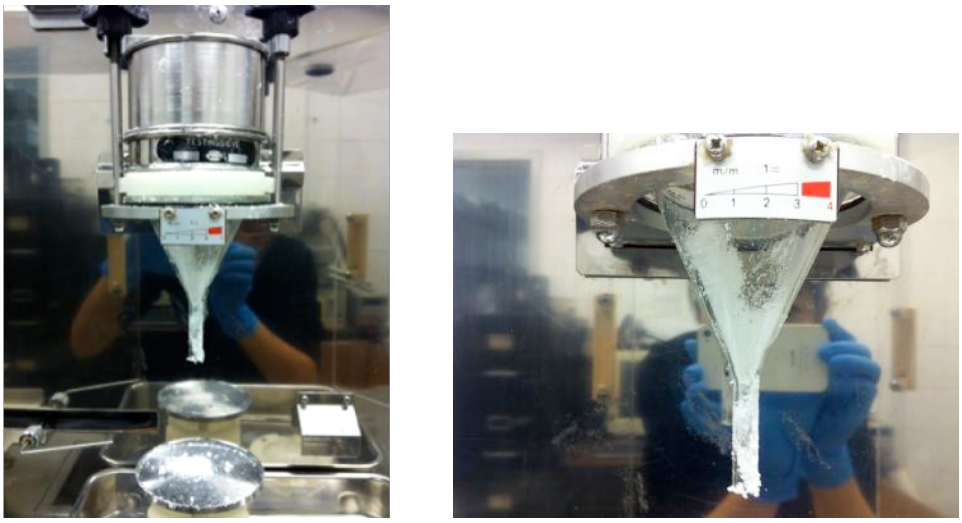

Figure 4.10 Inability to measure the angle of repose of milled APAP – blocked funnel.

Angle of repose of physical mixtures were also measured and shown in Figure 4.11. The original APAP/Soluplus has an angle of repose of 55 °, which is close to that of the original APAP alone, but the milled APAP/Soluplus has an angle of repose of 30 °, close to that of the Soluplus. The flowabilities of both original APAP and milled APAP were improved to some extent in the presence of Soluplus particles. Comparing to the angle of repose of original APAP/Soluplus, milled APAP/Soluplus physical mixture's angle of repose was reduced more, which may largely be due to that the milled APAP particles are able to attach on the surface of Soluplus particles and have less free APAP powders.

Figure 4.11 Angle of repose of original APAP/Soluplus (left) and milled APAP/Soluplus (right).

4.2 Quiescent Dissolution Behavior

4.2.1 Dissolution Behavior Observed during Hot Stage Microscopy

A hot stage was used to observe morphology evolution in conjunction with the optical microscope. Figure 4.12 shows morphology evolution of original APAP, milled APAP, Soluplus and physical mixtures (original APAP/Soluplus and milled APAP/Soluplus) at at 20 °C/min from 30 to 180 °C, conducted on a hot stage microscope. No change in shapes was observed in their morphologies during 30-80 °C, so, in Figure 4.12, the temperature range of their morphologies are presented from 80 to 180 °C. The glass transition temperature of Soluplus is 72.74 °C as shown in Figure 4.2, but the shape of Soluplus remains the same till 140 °C in Figure 4.12(c), which may imply that in the temperature range from 72.74 to around 140 °C, Soluplus is in its rubbery state. The original APAP and milled APAP alone in Figure 4.12(a) and (b) do not melt until reaching their melting point, but the presence of Soluplus promoted their dissolution at a temperature lower than their melting point, as shown in Figure 4.12 (d) and (e). In the

morphology evolution of original APAP/Soluplus (30/70), the APAP dissolved significantly in the molten polymer matrices at 160-170 °C, and completely disappeared after its melting temperature. Comparing to the morphology evolution of original APAP/Soluplus, milled APAP in its physical mixture with Soluplus almost completely dissolved into the molten polymer matrices at around 160 °C. At 140-160 °C, when the Soluplus are in liquid state, the morphologies on Figure 4.12 (e) show a thin layer of crystals, which is believed to be the milled APAP attached on the solid surface of Soluplus particles during dry blending. As Soluplus softens and proceeds thermally into the liquid state (dark circles), the APAP crystals are shown in the transmitted optical microscope, with cross-polarizer. The morphology evolutions under quiescent conditions offer a good and useful insight in the dissolution behavior of APAP with different particle sizes into the molten polymer, and can be used for the dissolution process under dynamic conditions.

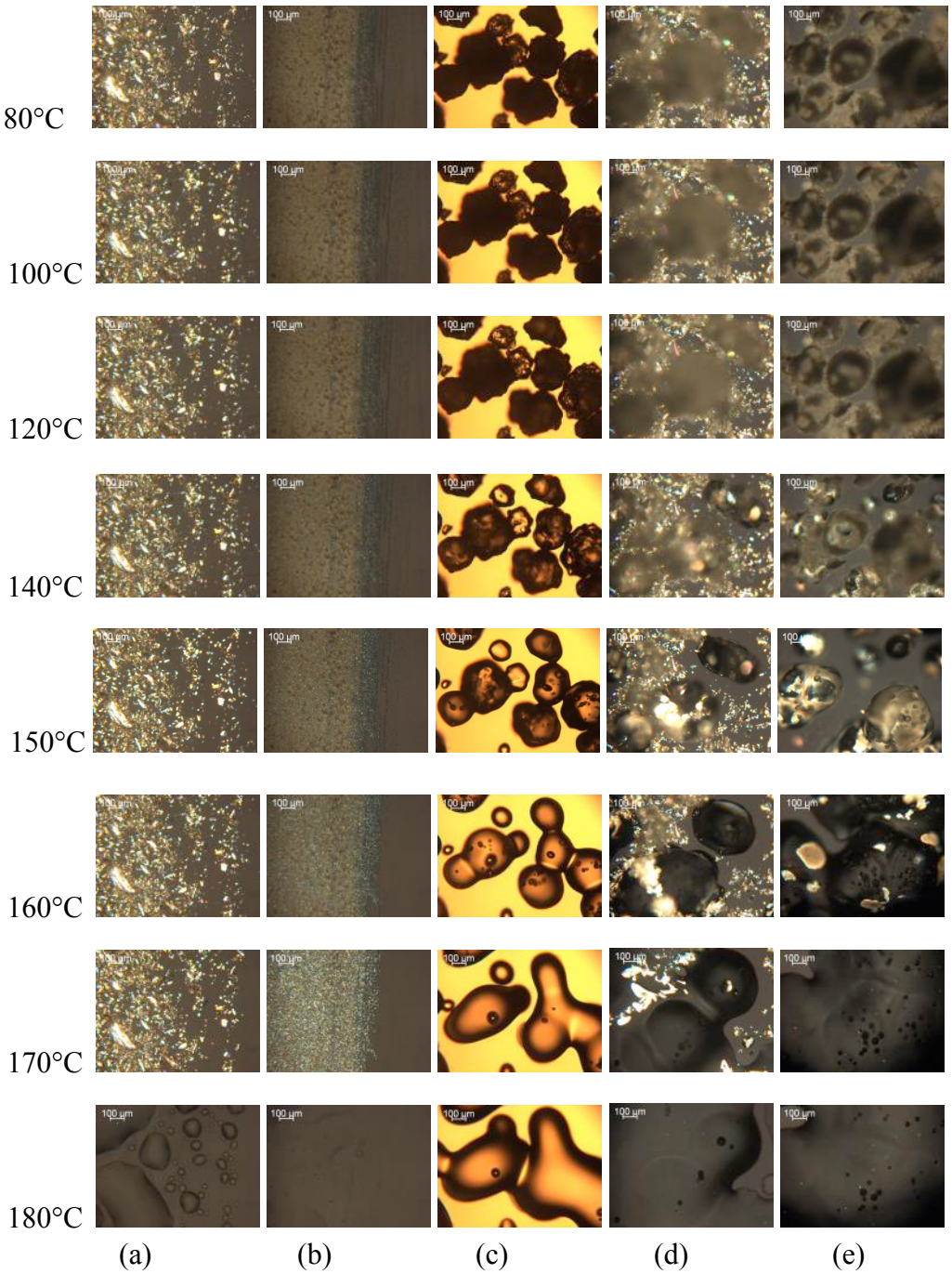

Figure 4.12 Transmission optical microscope morphology evolutions of original APAP with cross-polarizer (a), milled APAP with cross-polarizer (b), Soluplus without cross-polarizer (c), original APAP/Soluplus (30/70) with cross-polarizer (d), milled APAP/Soluplus (30/70) with cross-polarizer (e), during ramp heating.

According to the Noyes-Whitney equation (Equation 2.4), the dissolution rate is proportional to the particle's surface area.

$$\frac{\frac{dC_S}{dt}}{\frac{dC_L}{dt}} = \frac{A_{S,Total}}{A_L} = \frac{\frac{V_L}{V_S} \times A_S}{A_L} \tag{4.1}$$

where $\frac{dC_L}{dt}$ represents the dissolution rate of the original APAP particle; $\frac{dC_S}{dt}$ represents the dissolution rate of the milled APAP particle; A_L and V_L represent the surface area and volume of one original APAP; A_S and V_S represent the surface area and volume of the milled APAP.

In this case, if one original APAP particle is milled, the total surface area is increased and the dissolution rate as well as diffusion rate will be enhanced, correspondingly. The dissolution rate of milled APAP is roughly 23 times faster than the original APAP particles, as indicated by the following calculation, where the effect of the particle size on the mass transfer coefficient is neglected:

$$\frac{\frac{dC_s}{dt}}{\frac{dC_L}{dt}} = \frac{\frac{200 \times 30 \times 10}{5 \times 1 \times 0.5} \times 2(5 \times 1 + 1 \times 0.5 + 5 \times 0.5)}{2(200 \times 30 + 30 \times 10 + 200 \times 10)} \approx 23$$

The diffusion characteristic time can be estimated as:

$$\frac{t_{D_S}}{t_{D_L}} = \left(\frac{thickness_S}{thickness_L}\right) = \left(\frac{0.5}{5}\right) = \frac{1}{100} \tag{4.2}$$

where t_{D_S} is the diffusion characteristic time of milled API particles; t_{D_L} is the diffusion characteristic time of original API particles; $thickness_S$ and $thickness_L$ are the thickness of milled API particles and the original API particles, respectively.

The diffusion rate of milled API particles is enhanced by around 100 times, according to the calculation, which is very desirable from the point of view of being able to shorten the average residence time in the Co-TSE.

4.2.2 Dissolution Behavior on DSC

In Figure 4.13, the broad peak of the Physical Mixture (PM) curve from 70 to 175°C is related to the dissolution of APAP in the Soluplus matrices taking place during the heating step and the melting of APAP (H. Liu Ph.D Dissertation 2010). The peak at 175°C corresponds to the melting of the undissolved drug, which is very similar to the results of hot stage microscopy in Figure 4.12(d).

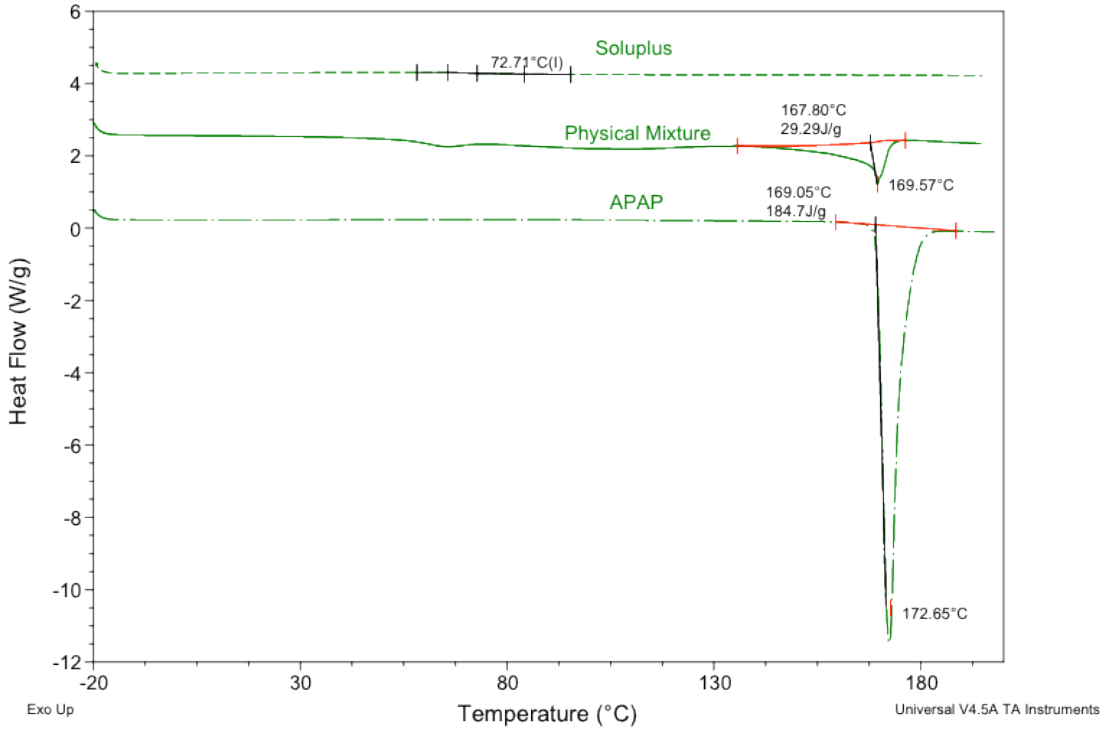

Figure 4.13 DSC curves of original APAP, Soluplus and their 30/70 physical mixture, at a heating rate of 20°C/min.

The melting enthalpy of APAP is about 184.7 J/g, determined by the universal analysis 2000 software. In the APAP/Soluplus (30/70) physical mixture, the dissolution enthalpy of APAP is 29.29 J/g. This corresponds to: 29.29 J/g × 100/30 = 97.63 J/g for dissolving APAP into Soluplus. If melting requires 184.7 J/g and dissolution requires 97.63 J/g then the hetero-contacts between APAP and Soluplus are energetically favored compared to the homo-contacts between APAP-APAP. In other words, the interactions between APAP and Soluplus, that are the inter-molecular "dispersion" forces, are larger than that between APAP particles.

Figure 4.14 presents the melting behavior of original APAP, milled APAP, the dissolution behavior of APAP in original APAP/ Soluplus (30/70) and milled APAP/Soluplus (30/70) in the DSC ramp at a heating rate of 20 °C/min. The enthalpies needed to melt the APAP with different particle sizes are almost the same, which indicates that the milling process did not destroy the crystalline structure of the drugs. For the original APAP/Soluplus (30/70), the melting peak, which corresponds to undissolved APAP, is larger compared with that of the milled APAP/Soluplus (30/70). That is probably due to more enthalpy needed to dissolve APAP left in the physical mixture. In the absence of any mechanical energy by the rotors, which results in deformation of compression of the packed PM, both the melting of excipient and dissolution of API by conduction were not completed before heated to the melting point of API. And the results of DSC ramp show that the particle size of API has an effect on their dissolution rate of drug into polymer matrices in the quiescent situation. These results are also close to the hot stage optical microscopy results in Figure 4.12 (a), (b), (d) and (e).

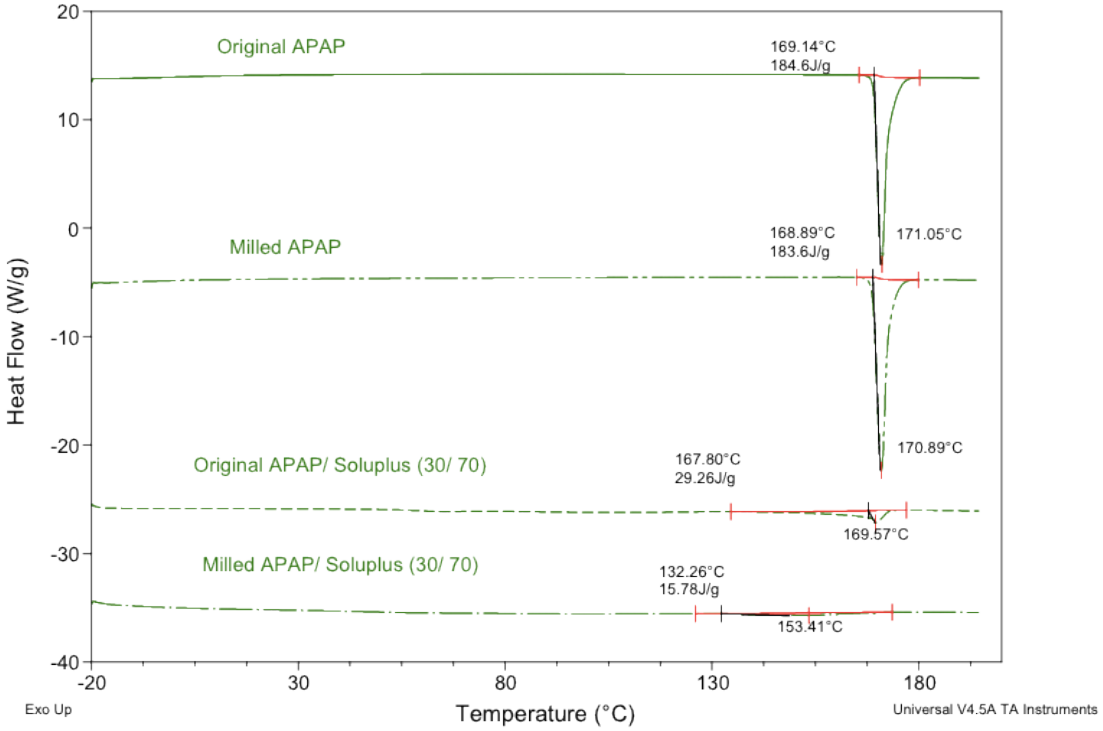

Figure 4.14 DSC ramps of original APAP, milled APAP, original APAP/Soluplus (30/70) and milled APAP/Soluplus (30/70), at a heating rate of 20 °C/min.

A DSC ramp mode was used to investigate the effect of heating rate on the melting and dissolution process under quiescent conditions. Figure 4.15 shows the melting process of APAP during heating steps. The peak at around 173 °C corresponds to the melting point of APAP. The heating rates were set at 5, 20, 50 °C/min, respectively. As expected, the heating rate slightly affects the melting temperature of APAP, since at high heating rate, 50 °C/min, the melting peak of APAP is 173.9 °C, but at low heating rate of 5 °C/min, the peak appears at 170.7 °C/min.

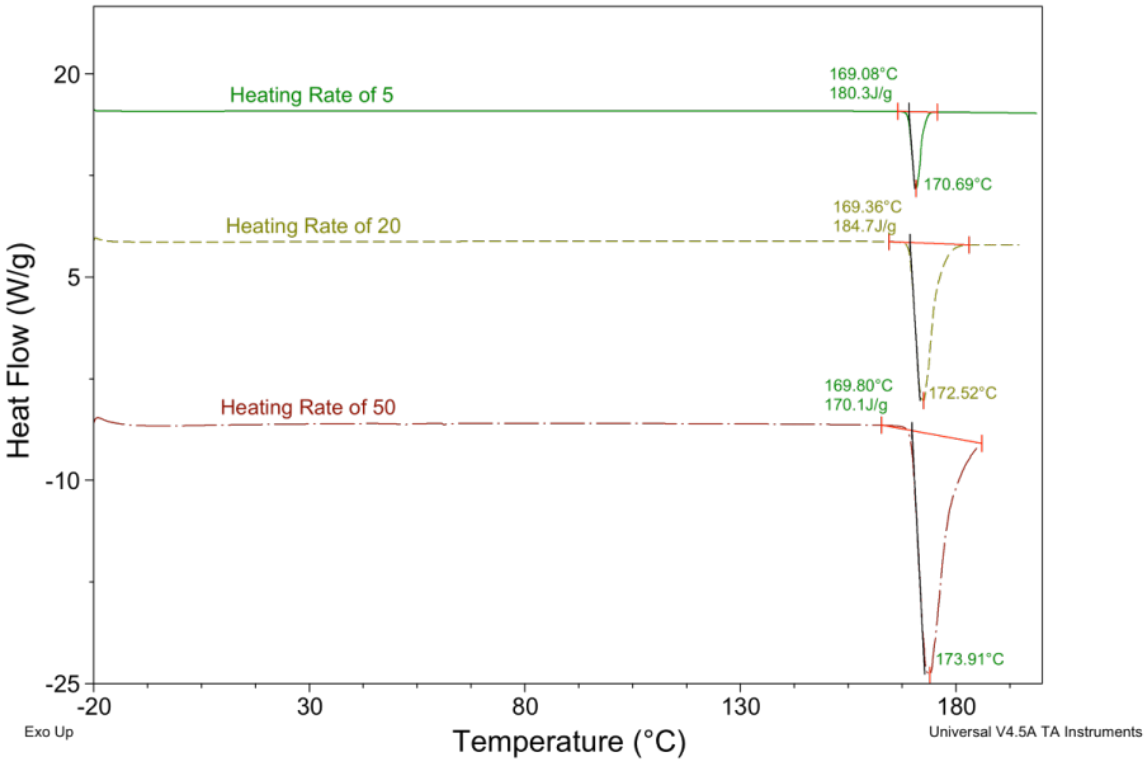

Figure 4.15 DSC ramps of APAP at heating rates of 5 °C/min, 20 °C/min and 50 °C/min.

DSC ramp heating responses of original APAP/Soluplus (PM 1#) at different heating rates were studied to investigate the dissolution process of APIs. The broad peak of the heating rate of 50 °C/min curve from 70 to 175 °C is related to the dissolution of APAP in the Soluplus matrices taking place during the heating step and the melting of APAP. The peak at 173 °C corresponds to the melting of the undissolved drug. For the condition of low heating rate, the APAP get dissolved gradually during the long heating step (40 min), the melting peak is smaller compared to that heated up at the high heating rate and, therefore, a short heating time (4 min). Comparing Figure 4.15 to Figure 4.16, the broad melting peak before the melting point of API is obvious in the presence of

excipient, which implies the dissolution of API in the polymer matrices during the heating step in DSC. Comparing the enthalpy differences in Figure 4.15 and Figure 4.16 at the same heating rate, the enthalpy needed during the heating step of DSC for APAP alone is much larger than that for the physical mixture, which, as mentioned above, indicates that the interaction between polymer Soluplus and API APAP is stronger than the interaction between APAP particles themselves.

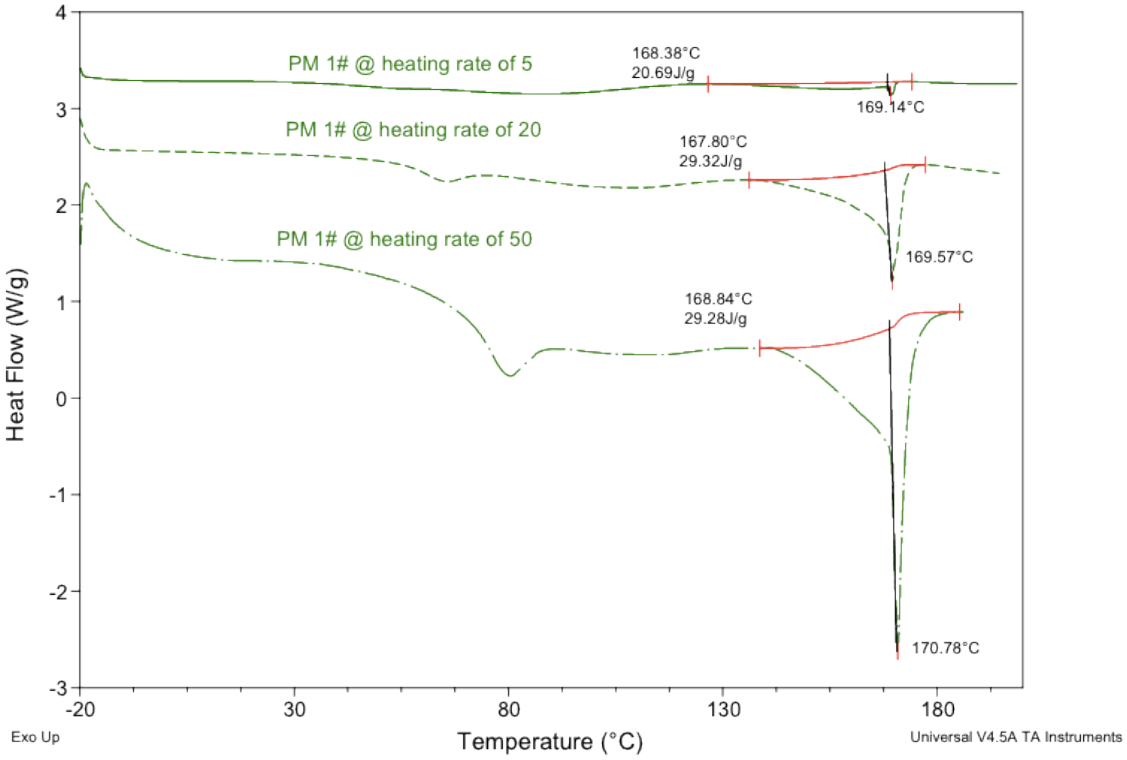

Figure 4.16 DSC ramps of original APAP/Soluplus (30/70) at heating rates of 5 °C/min, 20 °C/min and 50 °C/min.

4.2.3 Concluding Remarks

The original APAP in the physical mixture did not completely dissolve until 170 °C under quiescent conditions, conducted by the hot stage microscope. The onset temperature of the dissolution peak may provide an insight of minimum processing temperature of HME. Furthermore, the morphology evolution during ramped hot stage microscopy supports the dissolution analysis of ramped DSC results. Also, the effect of particle size on the dissolution of APAP into polymer matrices was investigated using the ramp mode of DSC instrument and hot stage optical microscope. The results show that the particle sizes of API affect the dissolution rate of the drugs into the polymer matrices under quiescent conditions, in the absence of any mechanical energy converted into heat. The milled APAP coated on the surface of Soluplus particles, increasing the contact area and thus enhance the diffusion and dissolution rates of APAP in to molten polymer matrices.

The dissolution of APAP into the Soluplus matrices was studied using the DSC at different heating rates, in which, the heating rate of 50 °C/min in the DSC ramp mode is most similar to that in the extrusion process, where the temperature jumps to 100 °C, the barrel set temperature. In that case, conduction melting is believed not to be the dominant factor affecting the dissolution process.

4.3 Batch Mixing

4.3.1 Morphology Observations

Figure 4.17 shows optical micrographs of batch mixer mixing samples taken at 90 s, 540 s. The heating rate was set 20 °C/min from 100 to 170 °C on the hot stage. The crystals inside the sample 90 s begin dissolving at 140 °C and disappear at 170 °C in the transmission optical microscopy of hot stage, which implies that the particle size of API was decreased during the batch mixing, but there is undissolved API. Sample 540 s fully melted at 140 °C, which is significantly lower than the melting temperature of APAP. The morphology observations show that APAP gets dissolved in Soluplus during the Brabender mixer mixing.

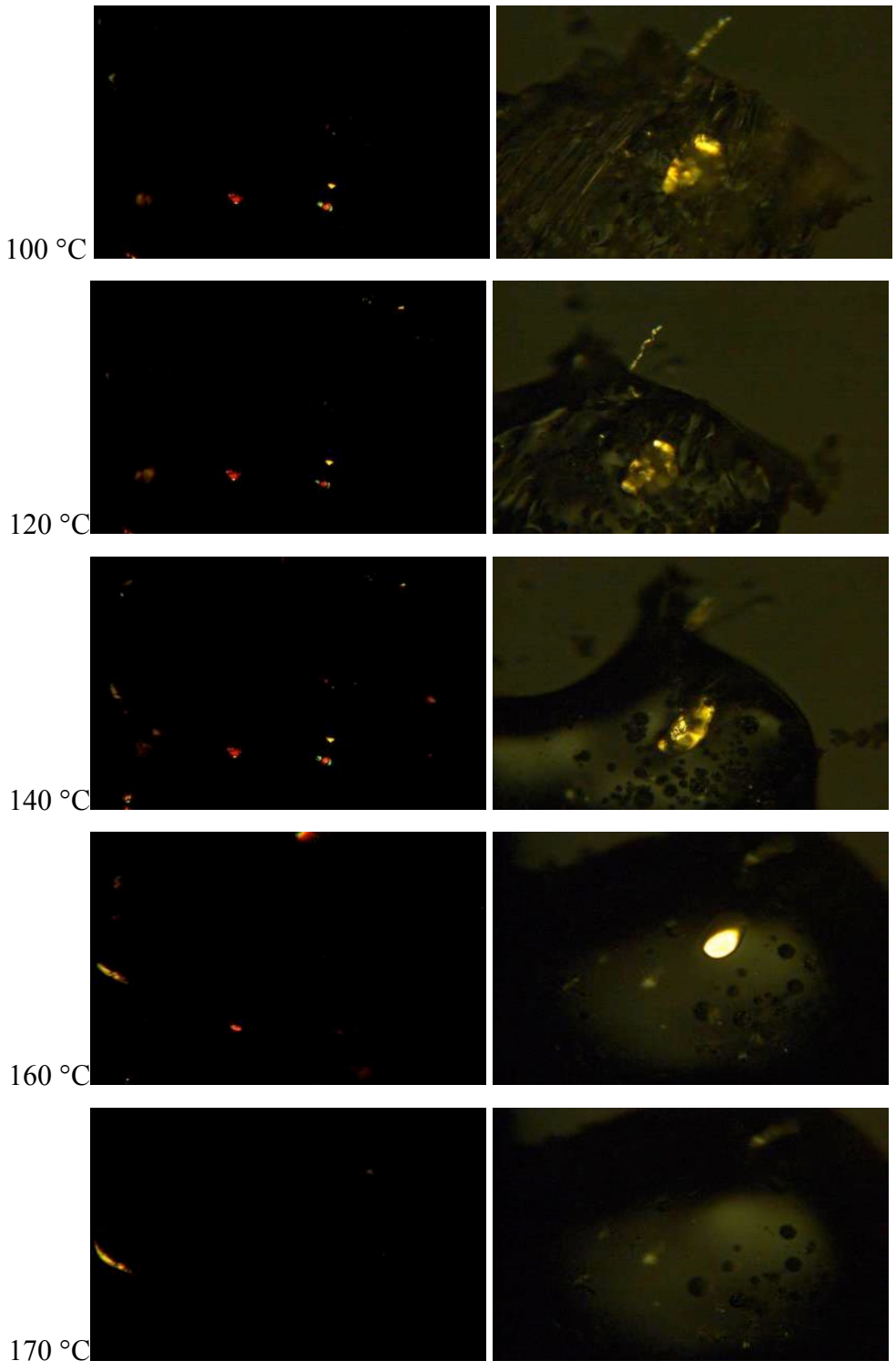

Figure 4.17 Transmission optical microscopy evolutions of original APAP/Soluplus (30/70) extrudates taken from batch mixer at 90 s and 540 s, with cross-polarizer, during ramp heating.

4.3.2 DSC Observations

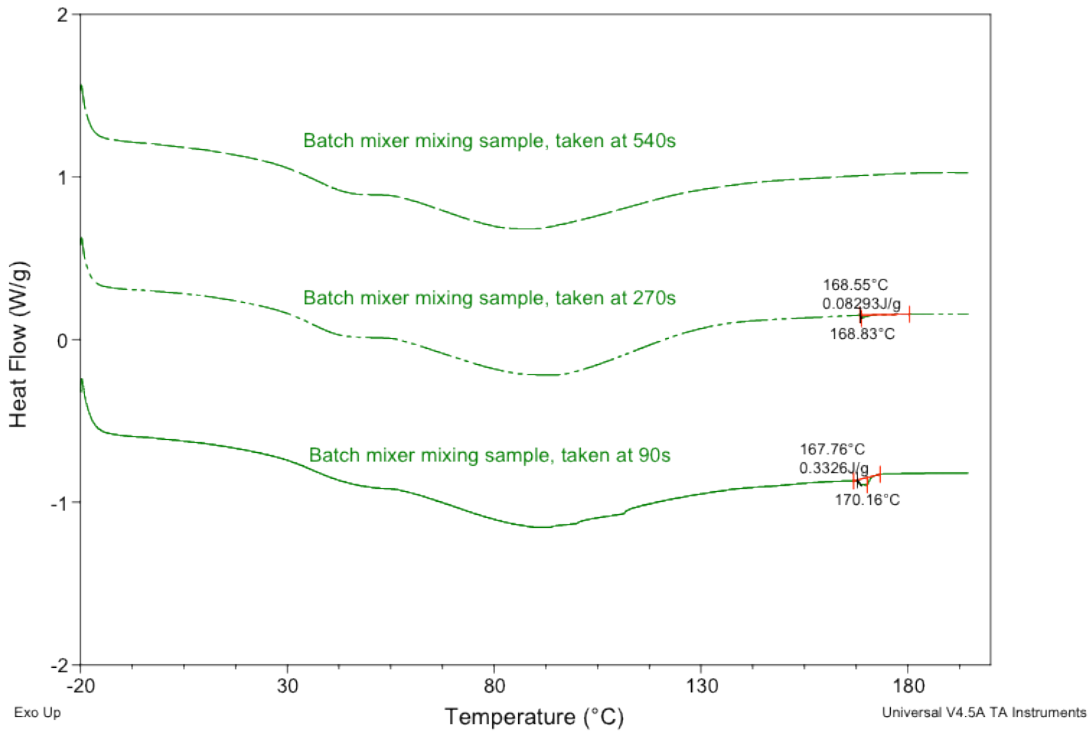

Figure 4.18 DSC curves of original APAP/Soluplus (30/70) extrudates taken from batch mixer at 90 s, 270 s and 540 s, at a heating rate of 20 °C/min.

Figure 4.18 shows the DSC curves for the samples taken from the Brabender mixer. The peak at 175 °C of sample 90 s implies the melting of crystalline APAP. At the scanning rate used, the peak at 175 °C is identical to the melting peak of APAP. But the peaks are too small to definitely prove that there are crystals left in the samples. For the 540 s sample, there is no melting peak at 175 °C, which implies that there is no detectable APAP crystal in the extrudate. This result may demonstrate that the rate of dissolution of APAP in the Soluplus molten matrices inside batch mixer at 100 °C is quite slow, roughly 8-9 min. This slow dissolution rate of APAP into Soluplus at 100 °C will present

problem during HME, conducted in the APV 15, where the average residence time is normally 2-3 min, unless mechanical energy and more effective mixing flows assist dissolution of APAP.

4.3.3 Concluding Remarks

The dissolution of APAP solid particles into molten Soluplus matrices was studied through processing the original APAP/Soluplus (30/70) in a batch mixer at different residence time, below the melting temperature of the API. The overall dissolution time of API into polymer matrices during batch mixing at 100 °C was around 8-9 min, which is much longer than the acceptable residence time for HME processes, which handle temperature sensitive APIs.

4.4 Co-rotating Twin-screw Extrusion

Two screws with a strong forward/reverse kneading blocks at positions KS20 and KS08, respectively, indicating the axial positions 20 and the eight diameters downstream, as well as one with only conveying elements (CS), shown in Figure 4.19, were used in this research to investigate their effects of on the dissolution of APIs with different particulate sizes during the extrusion process. The screws with kneading blocks have a unique capability of becoming fully filled, since the reverse kneading elements create a holdback. Consequently, axial flow and back mixing take place due to the expansion and contraction of each of the cross-sectional area pockets between a pair of kneading paddles and the barrel of fully intermeshing, co-rotating twin-screw extruders shown in Figure 4.20. Secondly, kneading blocks can induce distributive and dispersive mixing. Distributive mixing refers to stretching the interfacial area between components lacking a

cohesive resistance and distributing them uniformly throughout the product volume; by contrast, dispersive mixing refers to the process involving particle size reduction of cohesive particulate components. In the system studied, distributive mixing is induced by the expansion/contraction process of kneading block. The expansion/contraction process causes time-varying extensional and folding chaotic flows. Since the interfacial surface increases more rapidly in extensional flow than in shear flow, fully-filled kneading block flows create rapid distributive mixing. Dispersive mixing can be induced in the high-shear gap between the intermeshing kneading paddles and the barrel wall, which are desired for agglomerate breakup. Furthermore, kneading blocks can significantly increase the average residence time of the polymer/drug mixture (Liu 2010).

CS

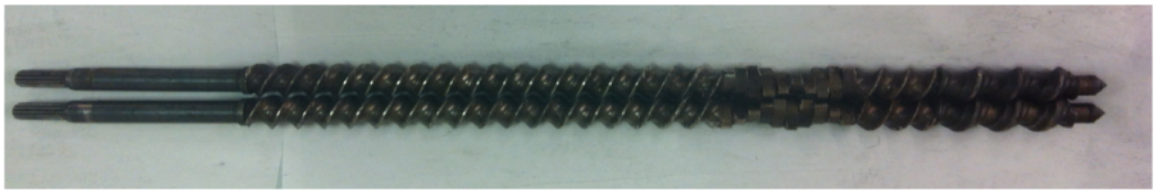

KS20

KS08

Figure 4.19 The three **s**crew configurations used in this research.

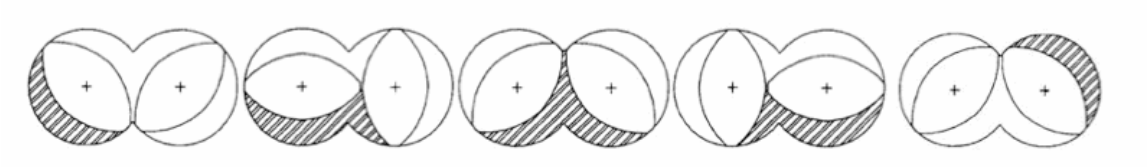

Figure 4.20 Snapshots of the repetitive expansion/contraction of each of the cross-sectional area pockets between a pair of kneading disks and the barrel of fully intermeshing, co-rotating twin-screw extruders. (Tadmor and Gogos 2006)

The raw materials were APAP and Soluplus with the original particle sizes of 100-200 μm and 300 μm, respectively. The APAP powders attached on the surfaces of the Soluplus after the two were physically mixed. When they were fed into the extruder, the Soluplus melted due to the high barrel temperature inside the extruder and the imposed viscous energy dissipation. As the Soluplus matrices got fully molten, it acts as a highly viscous solvent for the drug. The occurrence of dissolution of API is ascribed to the heat conducted from the hot barrel surface and the conversion of the mechanical energy supplied by the extruder motor taking place throughout the volume of the processed stream particularly in fully-filled regions. At the kneading block, distribution and dispersion of the particulates also occurs. The solid drug particles are suspended in a continuous polymer melt matrices, and start dissolving in the mass-transfer boundary layer between the drug and polymer particles because of the intermolecular forces between each other. This layer is continuously wiped away by the laminar distributive flow of the mixer and replaced by fresh polymer melt around each API particles. Finally, the API got fully dissolved into the polymer matrices.

4.4.1 Compressing and Grinding

Deformation of polymers and fracture of APIs may be induced by the fully-filled kneading blocks of the screws, which can possibly result in the reduction of API's particle size. The particle changes during HME were studied by compressing and grinding the raw materials using a press and a mortar and pestle. Optical microscopy was used to investigate structures of compressed tablets and to study the morphologies of the ground particles.

(I) Compressing

Soluplus tablets, APAP tablets and original APAP/Soluplus (30/70) tablets were made using the Laboratory press (Carver, Inc. Wabash, IN). The samples weighed 1.0 g each. The diameters of the Soluplus and original APAP/Soluplus (30/70) tablets are 2.6 cm and the thickness are 0.2, 0.18 cm, respectively. The APAP tablet had a diameter of 1.3 cm and a thickness of 0.5 cm. The tablet densities and the bulk densities are shown in Table 4.1. In Figure 4.20, the first tablet is the Soluplus, the second one is original APAP/Soluplus (30/70) and the third one is of the original APAP tablet. The original APAP tablet fell apart immediately after being taken out from the mode. The pressure applied was around 14,000 psi. For the Soluplus and the physical mixture, the pressure was stable after being set to the desired value.

Table 4.1 Bulk and Tablet Densities of Original APAP, Soluplus, and the 30/70 Physical Mixture

Density (g/cm^3)	**APAP**	**Soluplus**	**PM**
Bulk	0.33	0.52	0.61
Tablet	0.66	0.94	1.04

Figure 4.21 Images of Soluplus, original APAP/Soluplus (30/70) and APAP tablets.

The morphologies of Soluplus and APAP/Soluplus (30/70) tablets in Figure 4.22 were explored using an optical microscope. The Soluplus particles were packed solidly judging from the tablet surface in Figure 4.22, but there are gaps between particles. In the image of original APAP/Soluplus (30/70) tablet surface, the gaps are filled with the APAP powders. This agrees to the tablet densities shown in the Table 4.1, which indicates that the tablet density of original APAP/Soluplus (30/70) is higher than that of the Soluplus alone. Figure 4.23 shows the edge of the Soluplus tablet and the powders fell from the edge of the original APAP/Soluplus (30/70) tablet. The edge and surface of Soluplus tablet are identical in Figure 4.22 and Figure 4.23, but the original

APAP/Soluplus (30/70) tablet is loosened in the edge and powders fell from the edge as shown in Figure 4.23.

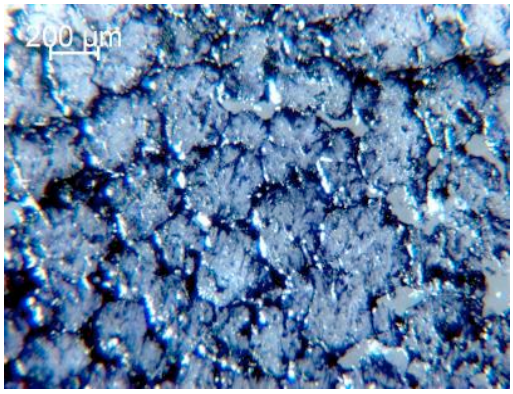

Colored Soluplus tablet

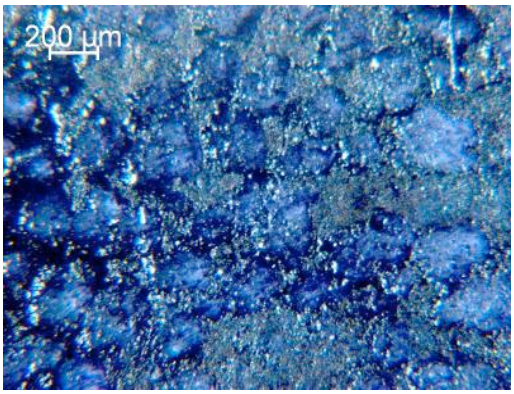

Colored original APAP/Soluplus (30/70) tablet

Figure 4.22 Reflection optical microscopy of colored surfaces of Soluplus tablet and original APAP/Soluplus (30/70) tablet.

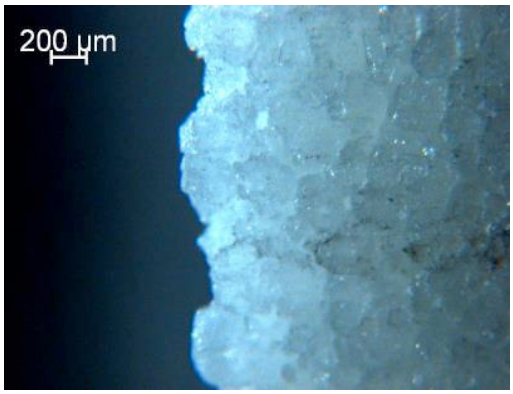

Uncolored Soluplus tablet edge

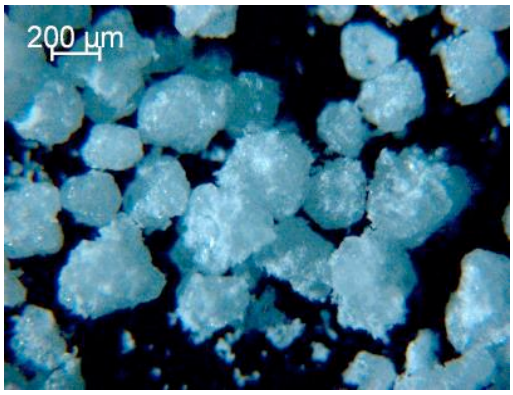

Uncolored powders separating from the original APAP/Soluplus (30/70) tablet

Figure 4.23 Reflection optical microscopy of uncolored Soluplus tablet edge and uncolored powders separating from the original APAP/Soluplus (30/70) tablet.

Figure 4.24 indicates that the large particle sizes of APAP in the compressed original APAP/Soluplus (30/70) tablet are around 100 µm, while the original APAP particles in Figure 4.5 are around 100-200 µm.

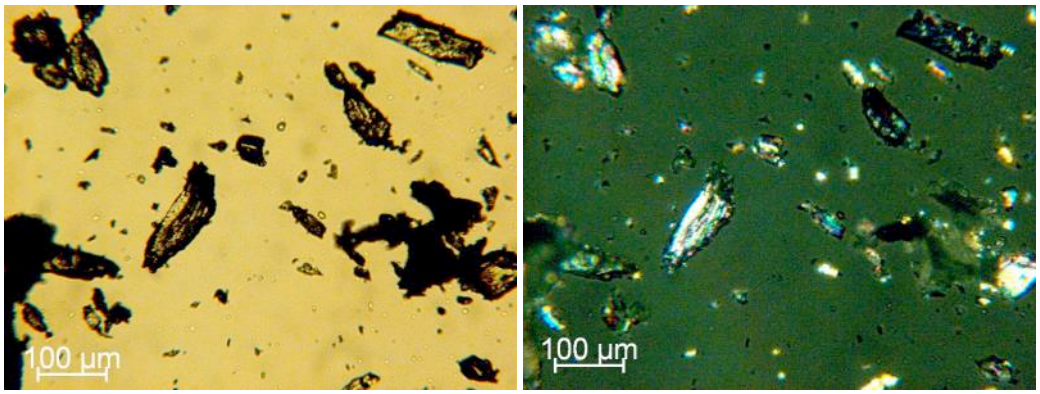

Figure 4.24 Transmission optical microscopy of APAP powders taken from the original APAP/Soluplus (30/70) tablets, without (left) and with (right) cross-polarizer.

Figure 4.25 shows the morphologies of APAP particles taken from APAP tablet. The large particles size shown in the image is around 100 µm. Comparing Figures 4.24, 4.25, and 4.26, the APAP particles were not broken significantly. The particles size of compressed/ground APAP is still much larger than the milled ones, which are around 5-10 µm.

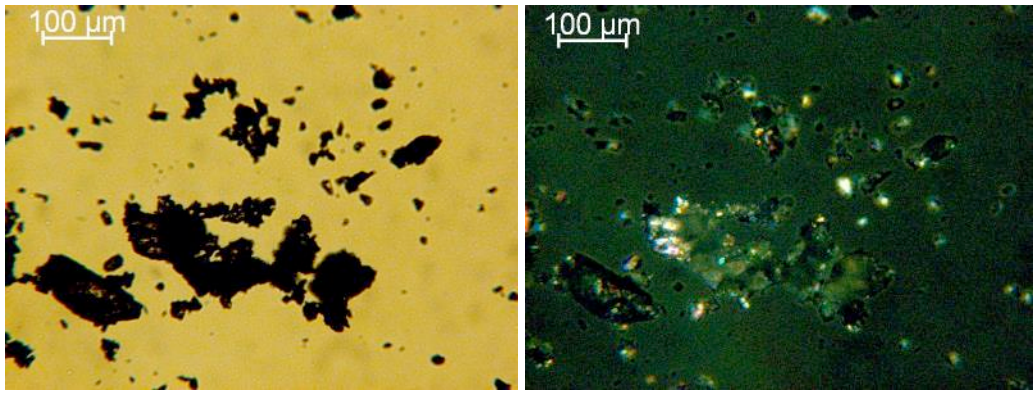

Figure 4.25 Transmission optical microscopy of APAP powders taken from the APAP tablet, without (left) and with (right) cross-polarizer.

(II) Mortar and Pestle Grinding

Figure 4.26 shows the ground APAP morphologies taken by the optical microscope. The size of the large particles is around 100 μm. This result is very similar to that happened in the compressing research.

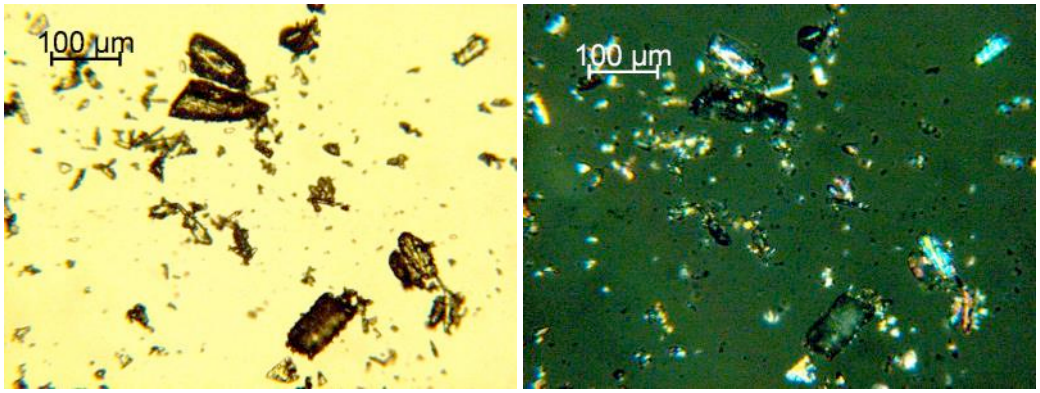

Figure 4.26 Transmission optical microscopy of ground APAP powders, without (left) and with (right) cross-polarizer.

When ground alone, the APAP particles were slightly broken and their particles were around 100 μm, as shown in Figure 4.26, which is similar to the compressing results. On the other hand, and the APAP particulate size in original APAP/Soluplus (30/70) was similar to that in the ground APAP/Soluplus (30/70) in Figure 4.27. This may because that during grinding, the large Soluplus particles created space for APAP to prevent it from being broken.

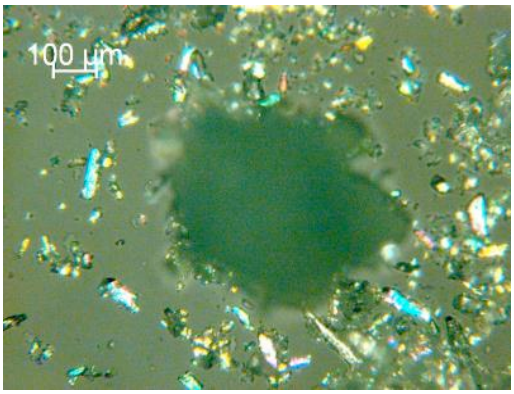

Figure 4.27 Transmission optical microscopy of ground original APAP/Soluplus powders, with cross-polarizer.

In this part of research, the effects of compressing and grinding on raw materials were studied. Similar effects may be induced by the forward/reverse kneading blocks during HME, where the free spaces are fully filled by raw materials, deformation and fracture of the raw materials may occur. Although the particles of Soluplus deformed and the APAP were broken to a small extent during compressing and grinding, as described above, the particle size of the broken APAP are much larger than the milled ones. It should be mentioned that, in the presence of Soluplus, the APAP particle size was not affected to any large extent. In other words, the fracture of APAP during HME will not affect the research on the effect of particle sizes on their dissolution rates into polymer matrices during HME.

4.4.2 Determination of Optimum Extrusion Temperature

Figure 4.28 shows the screws used to determine the optimum extrusion temperature. The offset (stagger) angle of the kneading paddles is 30°. For the forwarding kneading block, the larger offset angle, especially above 45°, leads to a smaller drag flow capability and

longer average residence time, because this configuration allows for larger pressure-driven “leak” backflows.

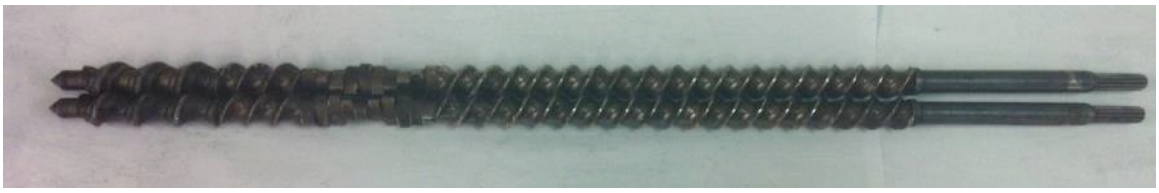

Figure 4.28 Screws used to determine the optimum extrusion temperature (KS20).

Figure 4.29 records the DSC curves of original APAP/Soluplus (30/70) extrudates processed at different setting temperatures, where the average residence time is around 3 min. There is no melting peak of APAP shown in the figure, which indicates that, in the extrudates, the APIs had fully dissolved into the polymer matrices at setting temperatures at 95 °C, 100 °C, 110°C and 120 °C, using KS20.

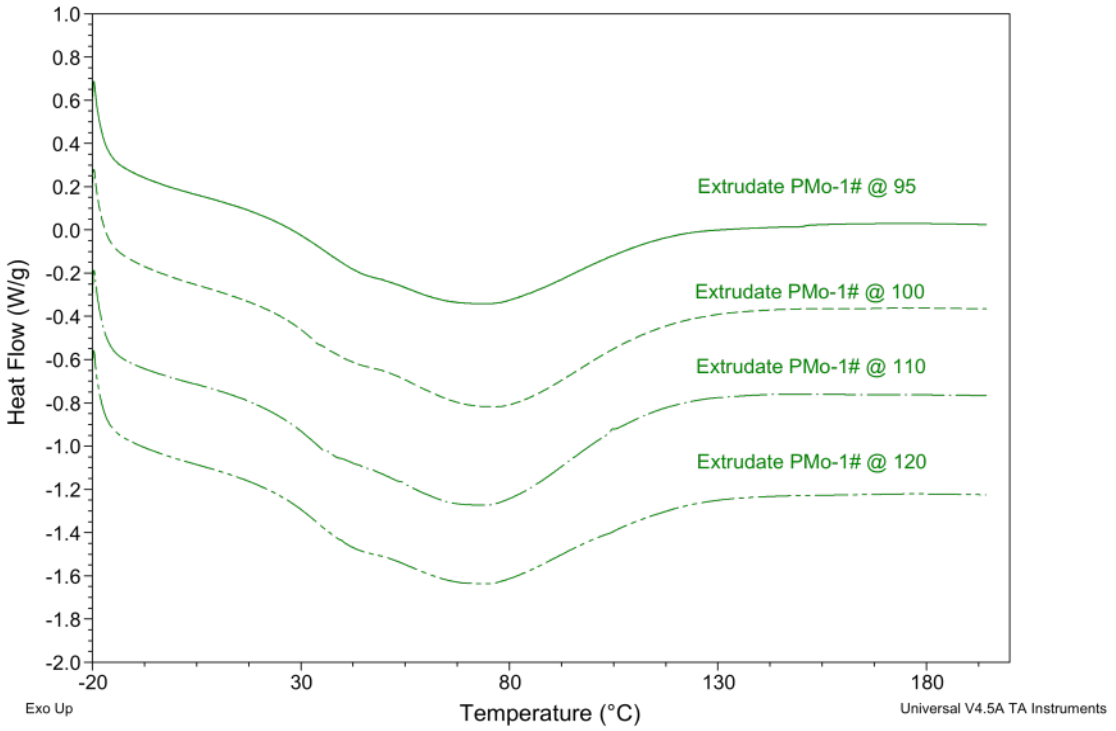

Figure 4.29 DSC curves of original APAP/Soluplus (30/70) extrudates processed at 95 °C, 100 °C, 110 °C and 120 °C, using KS20.

Figure 4.30 shows the screws, extruding original APAP/Soluplus (30/70), sampled out from the pulled screw carcasses after they reached the steady state. The average residence time is around 3 min. The powder physical mixtures were heated as they were fed into the extruder, which may decrease the PED, which increases with temperature rise. Figure 4.31 shows the DSC curves of samples taken along the screws. The broad peaks in the curves imply the further dissolution of APAP into Soluplus during the heating step of DSC, and the sharp peak in the curve of lobe 08 at 175 °C corresponds to the melting point of un-dissolved APAP in the extrudate. Because the kneading block was located in the second downstream half of the screws, the APIs got gradually

dissolved before reaching the intense kneading block, which may present a difficulty in the study of the effects of APIs' particulate sizes on their dissolution rates into molten polymer excipient matrices.

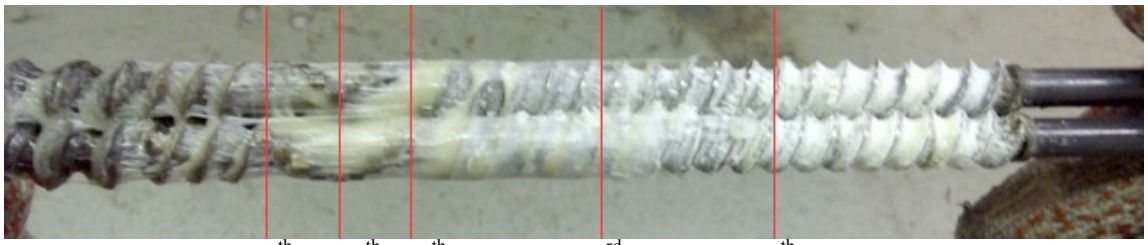

Figure 4.30 KS20 screws pulled out from the extruder, when extruding original APAP/Soluplus (30/70), T = 100 °C.

In Figure 4.31, the enthalpy needed to dissolve the API, which left in the 8th lobe, is $\frac{15.77 J/g}{29.29 J/g} = 53.84\%$ of that needed to dissolve the API in the physical mixture, which indicates that 46.16 % of total API has dissolved at the 8th lobe. Similar calculations can be carried out for other lobes, although the peaks are too small to definitely prove that there are crystals left in the extrudates at 25th and 30th lobe.

Table 4.2 Percentages of API Left in Original APAP/Soluplus Extrudates Taken at Different Lobes along KS20, T = 100 °C

Lobe Number	**PM 1#**	**08**	**13**	**19**	**25**	**30**
Enthalpy Absorbed (J/g)	29.33	15.77	3.045	1.491	0.9357	0.4418
Percentage of Total API Left	Assume 100	53.84	10.40	5.10	3.19	1.51

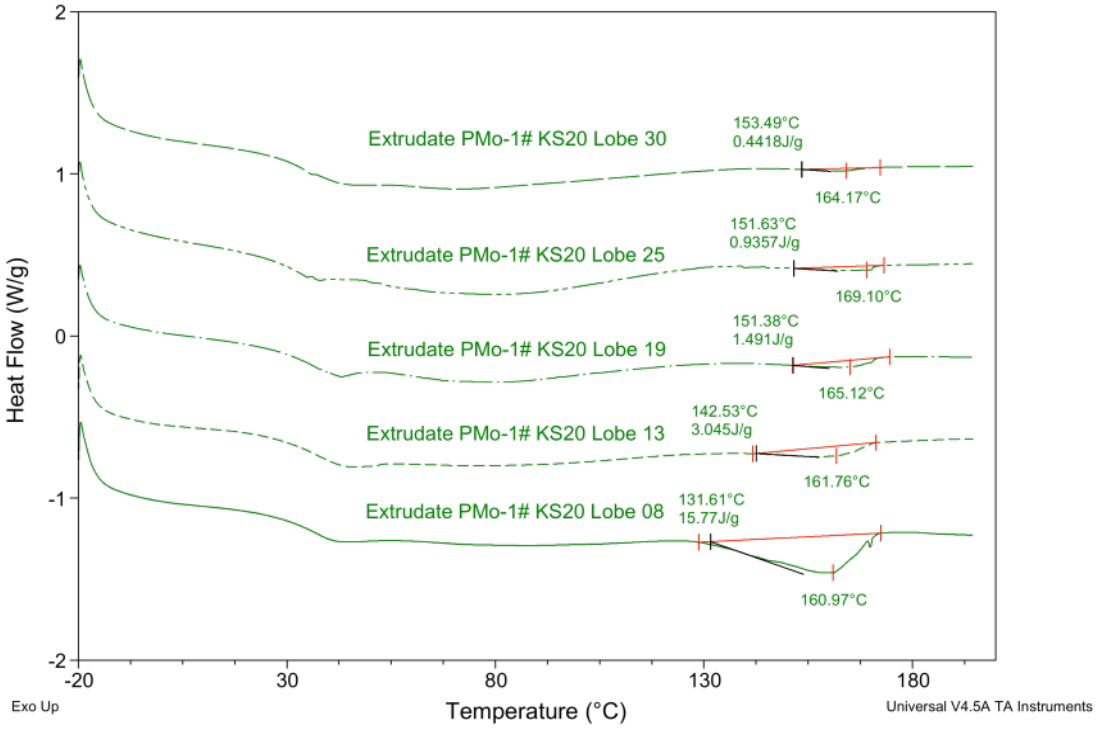

Figure 4.31 DSC curves of original APAP/Soluplus (30/70) extrudate samples taken along the KS20 screws, T = 100 °C.

4.4.3 Effect of Particles Size on the Dissolution Process of API, Conducted in the KS08 Configuration

Figure 4.32 shows the screw configuration (KS08) with kneading block used in this part of study to investigate the particles size on the dissolution rates of API. The kneading block is between the 8th and 18th lobes. As soon as the extrusion reached the steady state, the screws were pulled out from the extruder. Samples were taken along the screws and put between two pieces of metal to prevent APAP from further dissolution into the Soluplus matrices. Figure 4.33 shows the screws pulled out from the extruder when extruding the original APAP/Soluplus (30/70) and milled APAP/Soluplus (30/70), respectively. The kneading blocks were fully filled by physical mixtures.

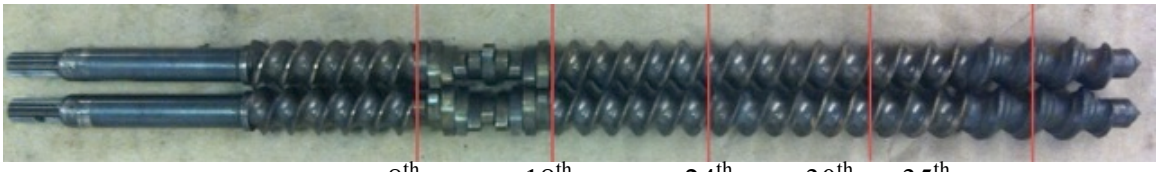

Figure 4.32 Screws used to investigate the effect of particle size on the dissolution process of API (KS08).

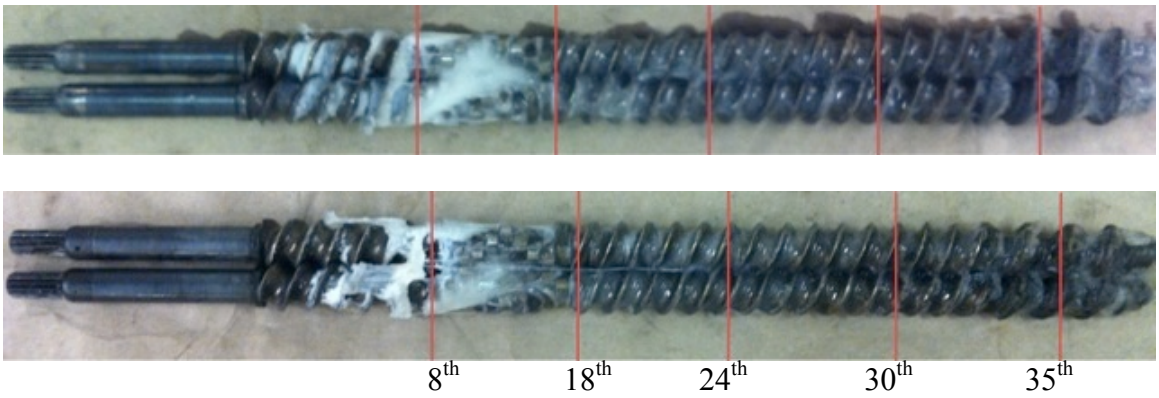

Figure 4.33 KS08 screws pulled out from the extruder, when extruding original APAP/Soluplus (30/70) and milled APAP/Soluplus (30/70), T = 100 °C.

Figure 3.34 presents optical microscopy, with cross-polarizer, of original APAP/Soluplus (30/70) and milled APAP/Soluplus (30/70) extrudate samples taken along KS08 screws. The extrudates were compressed into disks.

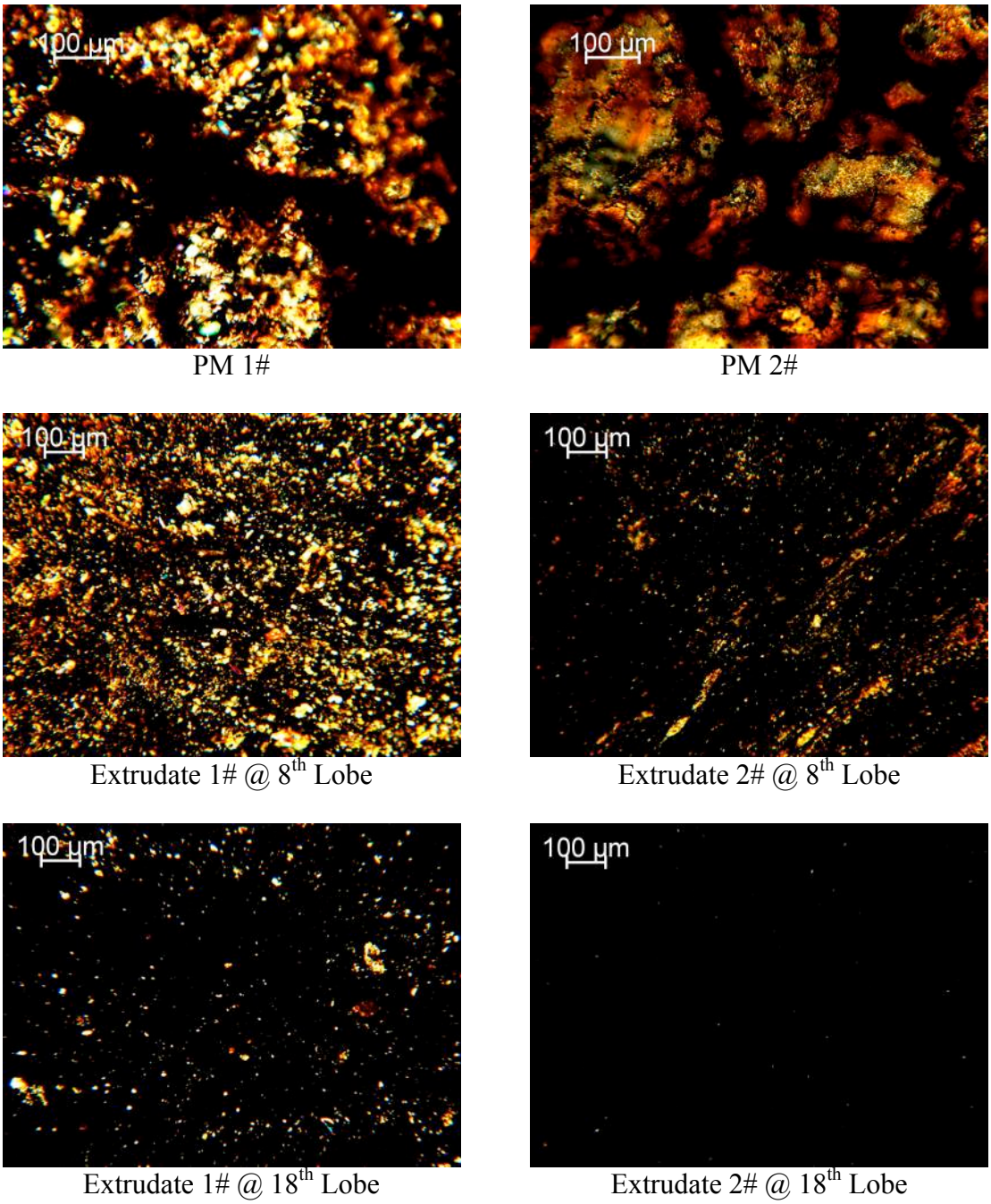

Figure 4.34 Transmission optical microscope morphologies of original APAP/Soluplus (30/70) (PM 1#) and milled APAP/Soluplus (30/70) (PM 2#) extrudate samples (Extrudate 1# and Extrudate 2#) taken along KS08 screws, with cross-polarizer, T = 100 °C.

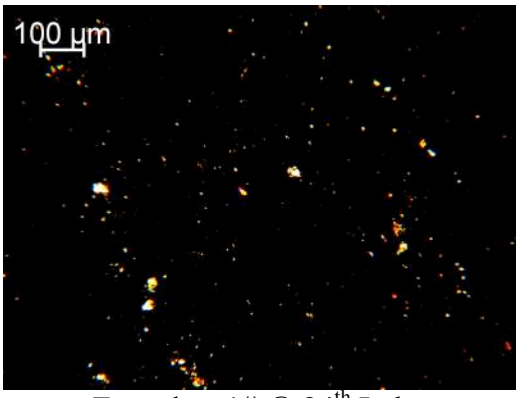

Extrudate 1# @ 24th Lobe

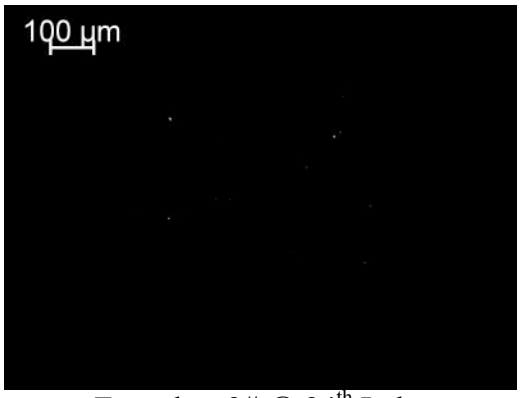

Extrudate 2# @ 24th Lobe

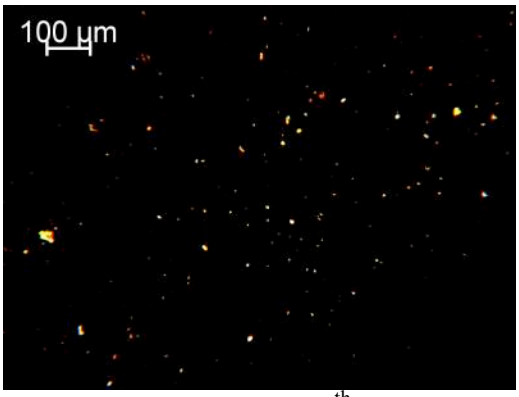

Extrudate 1# @ 30th Lobe

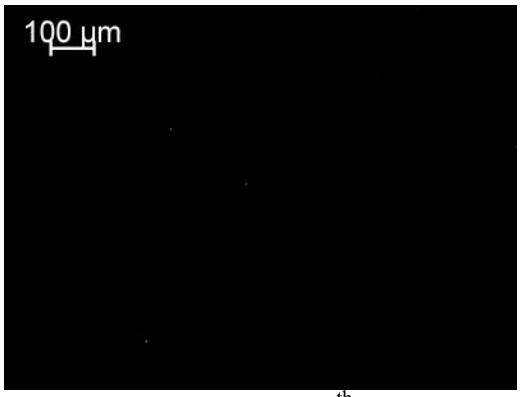

Extrudate 2# @ 30th Lobe

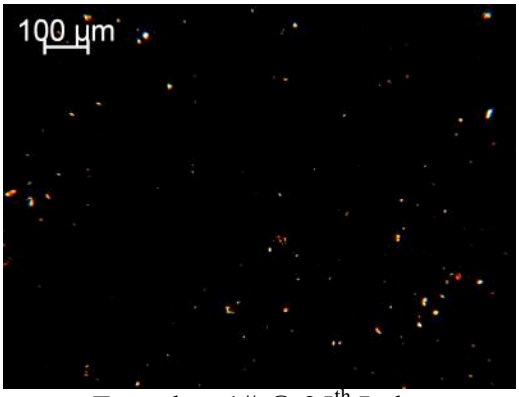

Extrudate 1# @ 35th Lobe

Extrudate 2# @ 35th Lobe

Figure 4.34 Transmission optical microscope morphologies of original APAP/Soluplus (30/70) (PM 1#) and milled APAP/Soluplus (30/70) (PM 2#) extrudate samples (Extrudate 1# and Extrudate 2#) taken along KS08 screws, with cross-polarizer, T = 100 °C. (Continued)

Figure 4.35 Time distribution along the KS08.

Physical mixtures were fed into the extruder conveying screw partially-filled feed section, where the predominant melting mechanism is conduction heating, and conveyed to the fully-filled kneading block in around 0.25 min. At the intense fully-filled kneading block, from the 8th lobe to 18th lobe, the mixture of solid Soluplus and drug particles were subjected to the very powerful, volume-wise melting mechanisms of PED and FED which melted the excipient particulates, which formed the continuous matrices for the suspended API particles. In the same fully-filled region efficient extensional flow created by the full kneading blocks plays a significant role in dissolving the API. The total average residence time in this region is around 2 min, which is two thirds of the total residence time. After the kneading block, the extrudate went through the conveying element with conduction heating and VED in roughly half a minute. Because of this experience, the amount, as well as the particle sizes, of original APAP in PM1# decreased markedly, but did not disappear after going through the kneading block region. In contrast, the milled APIs dissolved to a some extent before reaching the kneading block, and, after going through the kneading block, practically all the milled API particles were dissolved in the molten polymer matrices. According to the Noyes-Whitney

equation, the dissolution rate of milled APAP is expected to be more than 23 times higher than that of the original APAP, as mentioned earlier.

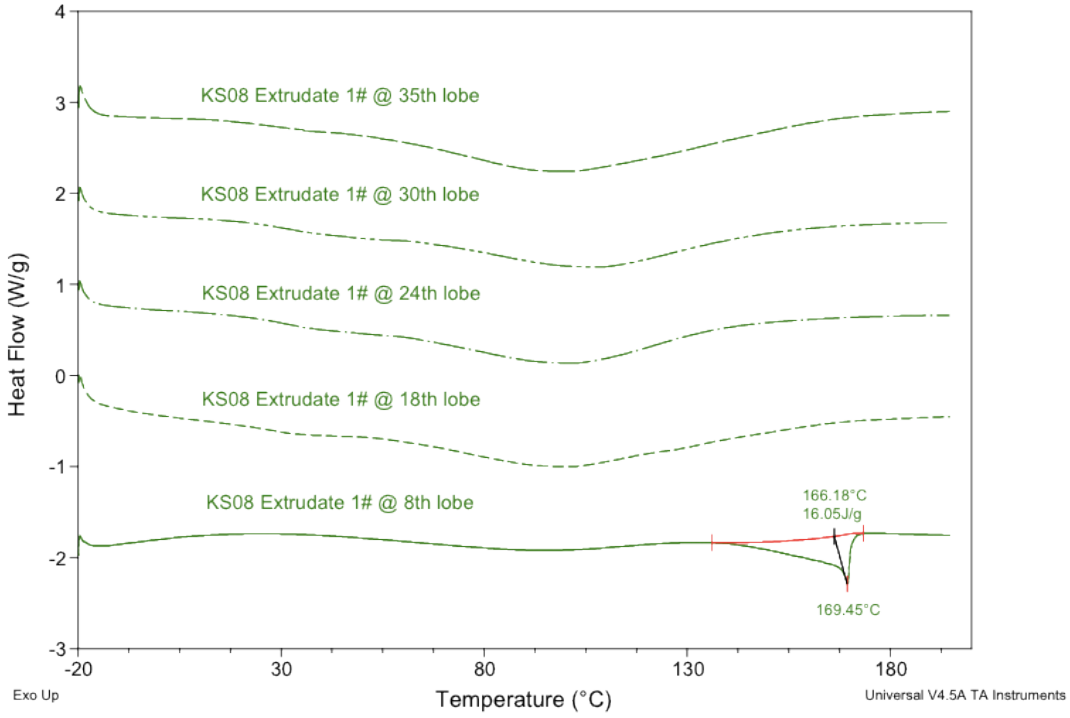

Figure 4.36 DSC curves of original APAP/Soluplus (30/70) extrudate samples (Extrudate 1#) taken at different lobes of KS08, T = 100 °C.

The percentage of APAP left in the extrudates at different lobes can be roughly calculated by dividing the amount of absorbed enthalpy of extrudates by that of the physical mixture, as mentioned before. For example, the DSC curve of Extrudate 1# at 8th lobe indicates that the enthalpy absorbed is 16.05 J/g, and the enthalpy absorbed data of PM 1#, from Figure 4.14, is 29.33 J/g. Thus, the percentage of total APAP left in the extrudate is

$$\frac{16.55}{29.33} = 54.7\%$$

There is around 55% of total APAP undissolved in the extrudate 1# at the 8th lobe. In fact, the extrudate samples were taken after stopping the instrument and pulling out the screws, but before, there might be more APAP in the extrudate during processing. This DSC ramp result is very close to the optical morphologies in Figure 4.34. After the kneading block, the amount of APAP left in the extrudate is either too small to be detected by the DSC ramp or APAP left in the extrudate dissolved during the heating step of DSC before the temperature reaching the melting point of APIs.

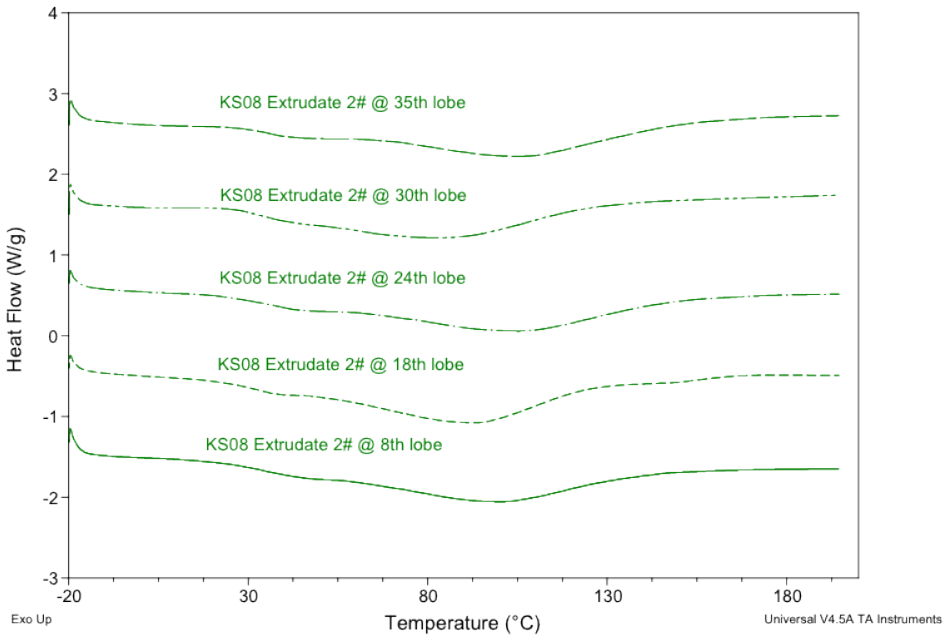

Figure 4.37 DSC curves of milled APAP/Soluplus (30/70) extrudate samples (Extrudate 2#) taken at different lobes of KS08, T = 100 °C.

The DSC curves of Exrudate 2# indicate that before the PM 2# reaching the kneading block of the screw, most of the APAP got already dissolved into the fully-filled molten polymer matrices. In this case, no melting peak was shown in the DSC curves for the extrudates taken along the screws.

4.4.4 Effect of Particle Size on the Dissolution Process of API, Conducted in the CS Configuration

Figure 4.38 shows the (CS) screws with only conveying elements used in this part of study to investigate the particle sizes on the dissolution rates of API. The average residence time in this case is only around 1 min, since there is no holdback and fully filled regions with backflows. As soon as the extrusion process reached the steady state, the screws were pulled out from the extruder. Figure 4.39 shows the screws pulled out from the extruder when extruding the original APAP/Soluplus (30/70) and milled APAP/Soluplus (30/70), respectively. The screws were partially filled by physical mixtures.

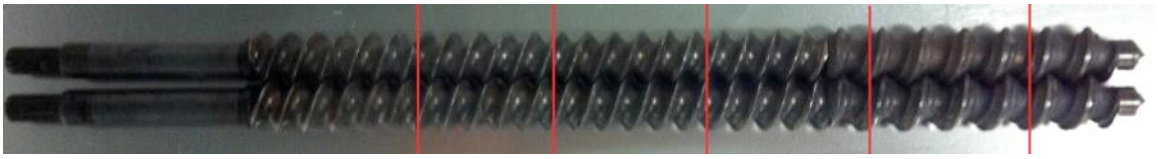

Figure 4.38 Screws used to investigate the effect of particle size on the dissolution process of API (CS).

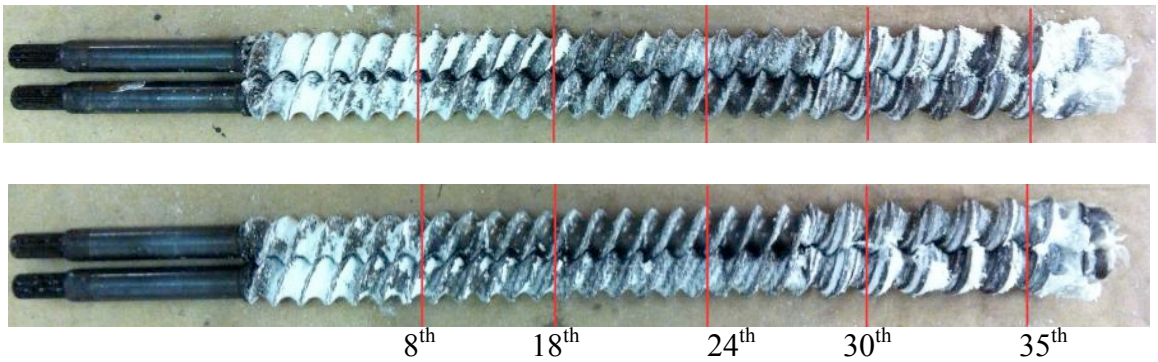

Figure 4.39 CS screws pulled out from the extruder, when extruding original APAP/Soluplus (30/70) and milled APAP/Soluplus (30/70), T = 100 °C.

Figure 4.40 presents optical microscopy, with cross-polarizer, of original APAP/Soluplus (30/70) and milled APAP/Soluplus (30/70) extrudate samples taken along CS screws. Extrudates were compressed into disks.

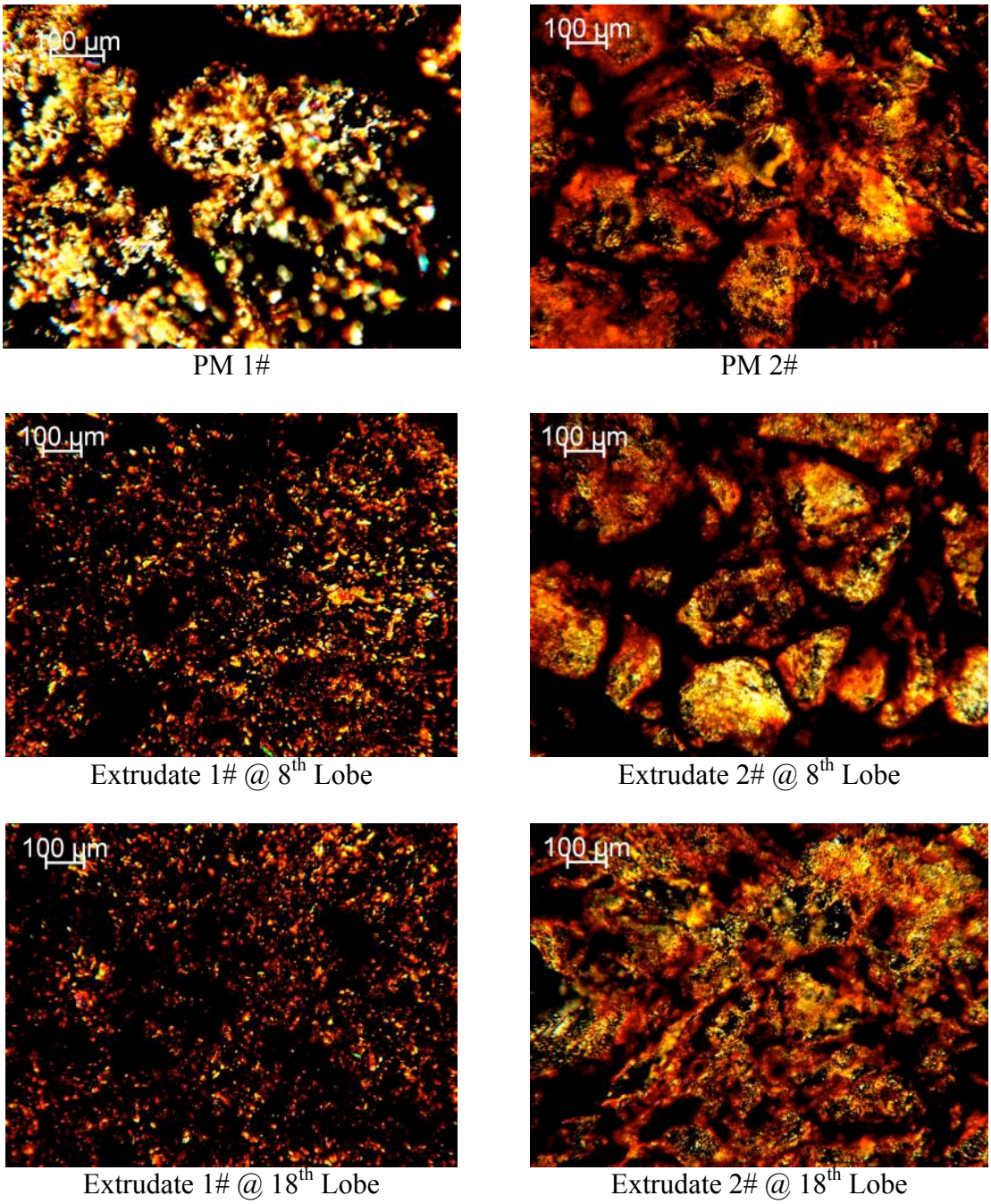

Figure 4.40 Transmission optical microscope morphologies of original APAP/Soluplus (30/70) (PM 1#) and milled APAP/Soluplus (30/70) (PM 2#) extrudate samples (Extrudate 1# and Extrudate 2#) taken along CS screws, with cross-polarizer, T = 100 °C.

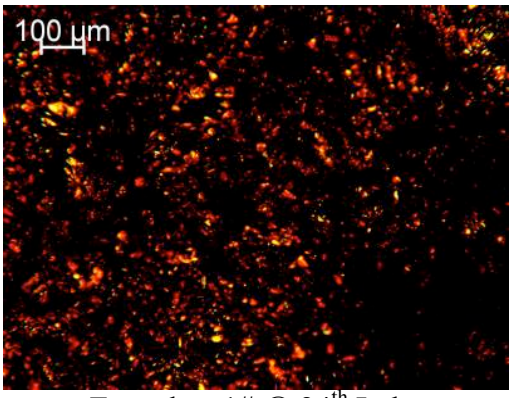

Extrudate 1# @ 24th Lobe

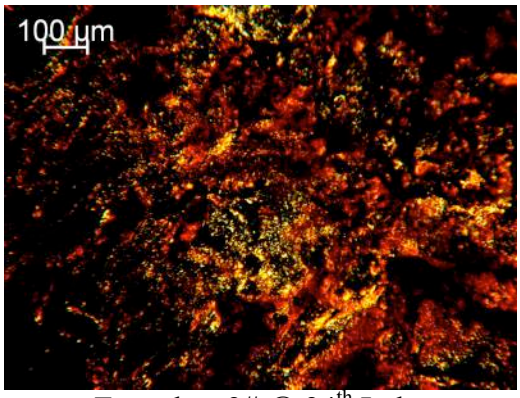

Extrudate 2# @ 24th Lobe

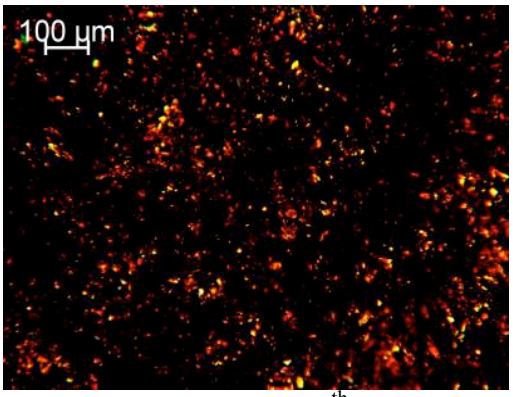

Extrudate 1# @ 30th Lobe

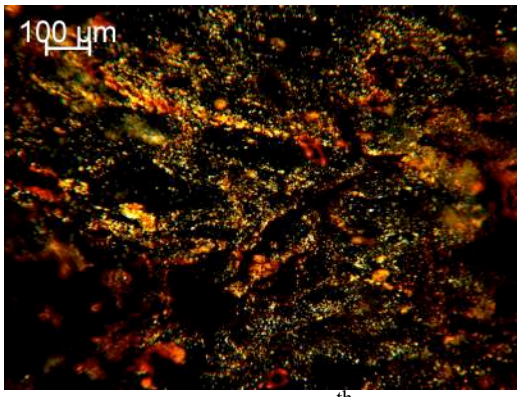

Extrudate 2# @ 30th Lobe

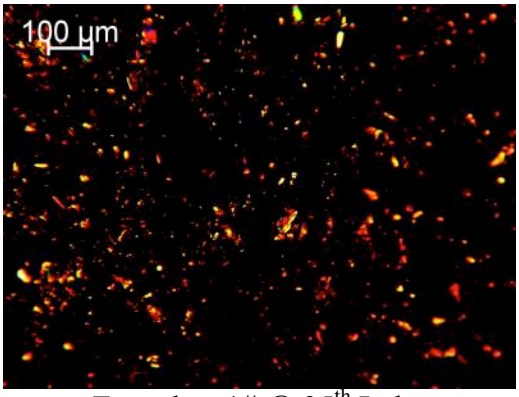

Extrudate 1# @ 35th Lobe

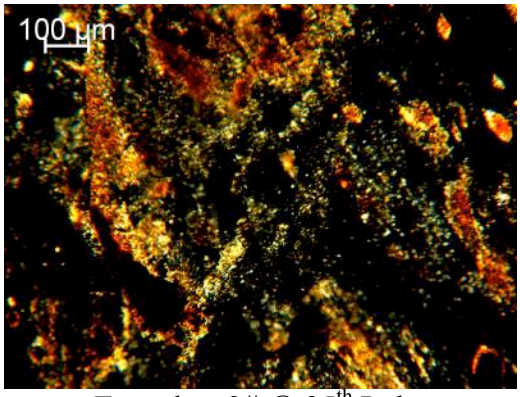

Extrudate 2# @ 35th Lobe

Figure 4.40 Transmission optical microscope morphologies of original APAP/Soluplus (30/70) (PM 1#) and milled APAP/Soluplus (30/70) (PM 2#) extrudate samples (Extrudate 1# and Extrudate 2#) taken along CS screws, with cross-polarizer, T = 100 °C. (Continued)

During the extrusion processing, using the CS crews, the melting of polymer and dissolving of API are mainly induced by the conduction heating along the barrel and screws. However, the materials residence time, using the conveying screws, is comparatively short, around 1 min, which is not long enough for melting and dissolution of the PMs. In addition, the screws with only conveying elements have limited ability to disperse and distribute APIs into the polymers. Thus, although the API was milled into a smaller particle size and thus the surface area is enlarged theoretically, their agglomeration will eliminate this advantage and delay the dissolution process of API in this case studied.

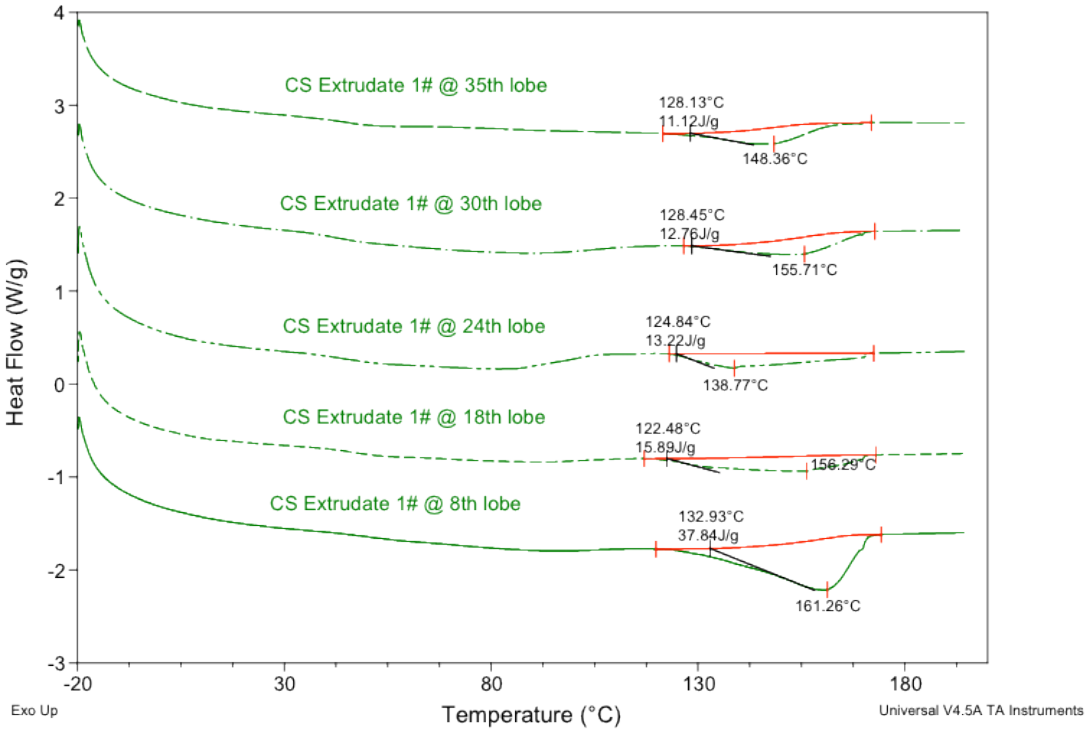

Figure 4.41 DSC curves of original APAP/Soluplus extrudate samples (Extrudate 1#) taken at different lobes along CS, T = 100 °C.

The enthalpy absorbed of the extrudate taken at the 8th lobe is larger than that of the physical mixture, which indicates that the APAP percentage in this extrudate is larger than that in the physical mixture. That may largely be due to the very poor flowability of APAP, whose angle of repose was measured, around 70 ° for the original size, but Soluplus has a low angle of repose around 10 ° and a very good flowability. Thus, APAP and Soluplus are conveyed differently during HME by the CS screws, leading to the segregation and inhomogeneous concentration along the screws.

The percentages of total APAP left in the extrudates 1# can be roughly calculated as described above. The results are listed in the Table 4.3.

Table 4.3 Percentages of API Left in Original APAP/Soluplus Extrudates (Extrudates 1#) Taken at Different Lobes along CS, T = 100 °C

Lobe Number	**PM 1#**	**08**	**18**	**24**	**30**	**35**
Enthalpy Absorbed (J/g)	29.33	37.84	15.89	13.22	12.76	11.12
Percentage of Total API Left	Assume 100	_	54.25	45.13	43.56	37.97

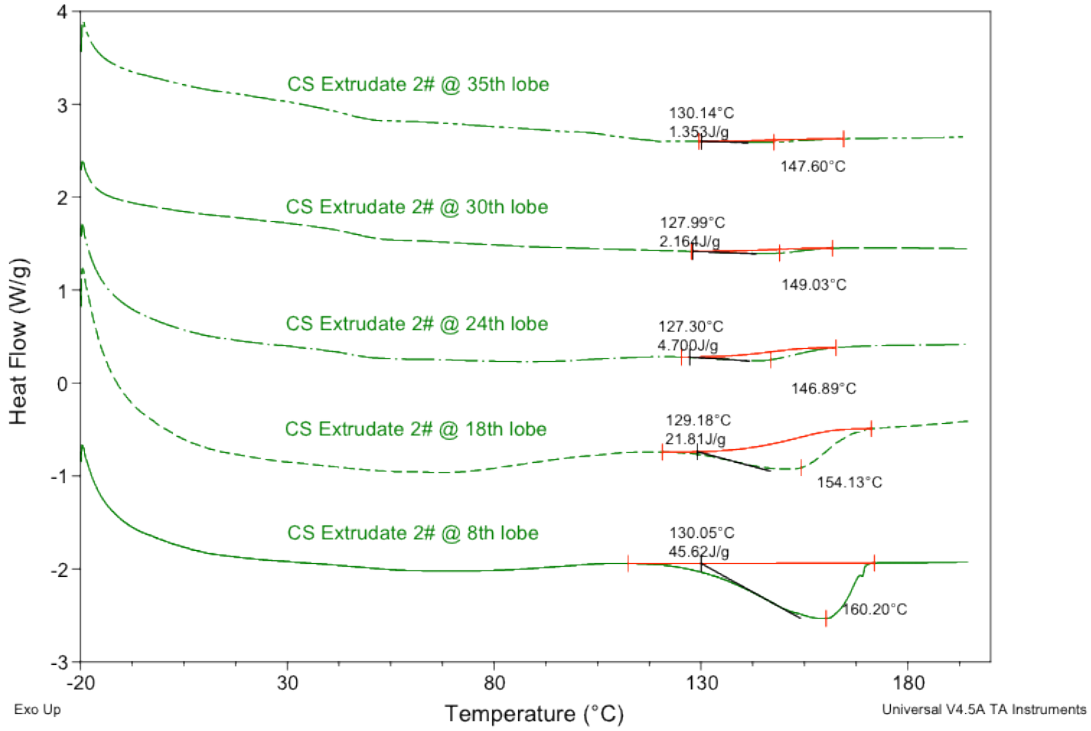

Figure 4.42 DSC curves of milled APAP/Soluplus extrudate samples (Extrudate 2#) taken at different lobes along CS.

Similarly, the percentages of total APAP left in the extrudates 2# are roughly calculated. The results are listed in the Table 4.4. The enthalpy needed to dissolve the APAP in the extrudates at 8th lobe and 18th lobe curves are larger than that needed to dissolve the APAP in the physical mixture, which indicates that their percentages of APAP are larger than that in the physical mixture. This is also due to the flowability differences between APAP and Soluplus.

Table 4.4 Percentages of API Left in Milled APAP/Soluplus Extrudates (Extrudates 2#) Taken at Different Lobes along CS, T = 100 °C

Lobe Number	PM 2#	08	18	24	30	35
Enthalpy Absorbed (J/g)	15.88	45.42	21.81	4.700	2.164	1.353
Percentage of Crystalline API Left	Assume 100	_	_	29.60	13.63	8.52

4.4.5 Concluding Remarks

Both of two physical mixtures, with different API particle sizes, were extruded using two different screw configurations, the KS08 and CS screws, with and without a fully-filled kneading block.

In KS20, where the kneading block located in the second downstream half of the screws, API particles gradually dissolved into the molten polymer matrix and the API particulate size was reduced before reaching the kneading block, which brings problems in the research of effects of API particle sizes on their dissolution rates in the molten polymer matrices.

APAP particles dispersed and distributed well when reaching the kneading block of KS08, according to the optical microscopy images. Most of the milled API, with particle sizes around 5-10 μm, dissolved in the fully-filled block of the screw, before going through the kneading block. For the original APAP in the physical mixture, its amount decreased dramatically after the kneading block, where the residence time is around 3 min. However, co-rotating twin-screw extruder with kneading block may have a chance to burn the materials because of the high processing temperatures and the laminar

flow heating due to viscous energy dissipation. As long as operated at an appropriately temperature, together with the occurrence of PED and FED, it is good for dissolving the API into the polymer excipient matrices.

The residence time in the extruder, using screws with only conveying elements, is roughly 1 min, which is not long enough to promote the melting and dissolving of the physical mixture, as shown in the figures of DSC ramp and optical morphology. In addition, conveying screws, where there is no PED and little FED, exhibit limited ability to disperse and distribute the API agglomerates. They also heat the processed physical mixture *only by conductive heating*, which for the short residence time results only in gradual and probably incomplete melting segregation occurred in both physical mixtures. The API agglomerates may prevent their dissolution in the molten polymer matrices, and what's more important is that they may eliminate the advantage of large surface area of milled API particles.

CHAPTER 5

SUMMARY AND FUTURE WORK

The research in this thesis has focused on the effect of the particle size of the API on their dissolution rate in the molten polymeric excipient during hot melt extrusion. Extrusion was conducted in the co-rotating twin-screw extruder using different screw configurations. Acetaminophen (APAP) and amphiphilic polyvinyl caprolactam-polyvinyl acetate-polyethylene glycol graft copolymer (PVCap-PVAc-PEG) (Soluplus®) were chosen as the model API and water-soluble polymer excipient. A fluid energy mill (FEM) was used to reduce the API particle sizes. TGA and DSC were used to characterize the thermal properties of processed samples. SEM and optical microscope were employed in the morphologies studies.

Based on the Noyes-Whitney equation, the dissolution rate of the milled APAP is expected to be much faster than the original APAP. Furthermore, since the milled APAP coated on the Soluplus particles, thus increasing the contact area, the diffusion and dissolution rates are further enhanced.

Under quiescent conditions, the APAP in the PM does not melt until 170°C conducted by the hot stage microscope. The onset temperature of the dissolution peak may provide an insight of the minimum processing temperature for HME. According to the DSC ramp traces, the particle size of API affects their dissolution rate into the polymer matrices. By using the DSC ramp behavior at high heating rate, 50 °C/min, which is similar to that in the extrusion process, where the temperature may quickly jump to 100°C from ambient in less than a minute, when PED and FED dominate in the fully-filled regions, and conductive melting is not the dominant heating mechanism.

When extruding the physical mixture in a batch mixer below the melting temperature of the API, it took about 9 min for all API dissolved into the polymer matrices, indicating that, under the conditions used the batch mixer did not supply enough mechanical energy and adequate mixing flows for complete dissolution in less than 2-3 minutes, needed for HME.

When extruding using the KS20 screws, where the kneading block is located in the second half of the screw, the APIs got gradually dissolved before reaching the intense kneading block.

The effect of particle sizes of APIs on their dissolution rates into the molten polymer matrices were explored using the KS08 and CS screws. When extruding using KS08, the APAP particles got dispersed and distributed well when reaching the kneading block of KS08, according to the optical microscopy. Most of the milled API, with particle sizes around 5-10 μm, dissolved in the fully-filled block of the screw, before going through the kneading block. For the original APAP in the physical mixture, its amount decreased dramatically because of the kneading block. Although care has to be taken with co-rotating twin-screw extruders having kneading blocks not to degrade the processed materials because of the generation of high melt temperatures due to PED and FED for melting and VED subsequently, it is good for dissolving the API into the polymeric excipient matrices. This can be achieved by properly choosing the intensity of the holdback generated by the reverse element number and stagger angle. When the first is reduced and the second is increased the heat generation rate is diminished. Finally, co-rotating twin-screw extruder with only conveying elements works only as the single screw extruder, where there is no PED and little FED. The dissolution is delayed for all

the API sizes used in this work, so that such screw configuration is inadequate for the original size and milled-APAP/Soluplus systems studied.

It is believe that, as future work, two areas are suggested by this thesis and worth pursuing:

First, the milled API (10 μm) particles dissolve very well, compared with the original APAP (100 μm), when extruded using screws with a fully filled kneading block at 8-18 lobes, and when the total residence time is roughly 3 min. On the other hand, there is the possibility of API agglomeration with particles of this size, especially at higher API concentrations. Thus, the dissolution rates of more particle sizes (20 μm, 30 μm…) should be investigated using the same co-rotating twin-screw element design, to find the optimum particle size, which can increase the contacting surface area between APIs and polymer, but prevent APIs from aggregating.

Reverse screws or reverse kneading elements in co-rotating twin-screw extruder create a filled section to pack particulates to undergo repeated volume-wide deformations, and thus create FED and PED. The residence time, PED as well as FED increase with the number of backward elements, which presents more of a danger for thermal degradation of the API. Thus, screws with fewer reverse kneading elements, such as 7F/3R instead of 5F/5R, can be explored to dissolve APIs with small particle sizes in order to reduce the chance of burning APIs during hot melt extrusion.

REFERENCES

A. Forster, J. Hempenstall, I. Tucker and T. Rades (2001). Selection of Excipients for Melt Extrusion with Two Poorly Water-soluble Drugs by Solubility Parameter Calculation and Thermal Analysis. Int. J. Pharm. (226):147-161.

A. Noyes, W. Whitney (1897). The Rate of Solution of Solid Substances in their Own Solutions. J. Am. Ceram. Soc. (19): 930-934.

C. Bruce, K.A. Fegely, A.R. Rajabi-Siahboomi, J. W. McGinity (2007). Crystal Growth Formation in Melt Extrusates. Int. J. Pharm. (341): 162-172.

C. Leuner, J. Dressman (2000). Improving Drug Solubility for Oral Delivery Using Solid Dispersions. Eur. J. Pharm. Biopharm. (50): 47-60.

C.G. Gogos, H. Liu, P. Wang, 2012. Laminar Dispersive and Distributive Mixing with Dissolution and Application to Hot-melt Extrusion, in: Douroumis, D. (Ed.), Hot-melt Extrusion: Pharmaceutical Applications. John Wiley & Sons Ltd., UK.

C.G. Gogos, Z. Tadmor, M.H. Kim (1998). Melting Phenomena and Mechanisms in Polymer Processing Equipment. Adv. Polym. Technol. (17): 285-305.

D.J. Greenhalgh, A.C. Williams, P. Timmins, P. York (1999). Solubility Parameters as Predictors of Miscibility in Solid Dispersions. J. Pharm. Sci. (88): 1182-1190.

D.Q.M.Craig (2002). The Mechanisms of Drug Release from Solid Dispersions in Water-soluble Polymers. Int. J. Pharm. (231): 131-144.

E.V.Thompson, 1985. in: H.F. Mark, N. Bikales, C.G. Overberger, G. Menges, J.I. Kroschwitz (Ed.), Encyclopedia of Polymer Science and Engineer, 2nd ed. Wiley-Intersicence, New York, NY. 16: 711-747.

G. Terife, P. Wang, N. Faridi, C.G. Gogos (2012). Hot Melt Mixing and Foaming of Soluplus® and Indomethacin. Polym. Eng. Sci. 52(8): 1629-1639.

G.R. Lloyd, D.Q.M. Craig, A. Smith (1997a). An Investigation into the Melting Behavior of Binary Mixes and Solid Dispersions of Paracetamol and PEG 4000. J. Pharm. Sci. (86): 991-996.

G.R. Lloyd, D.Q.M. Craig, A. Smith (1997b). An Investigation into the Production of Paracetamol Solid Dispersions in PEG 4000 using Hot Stage Differential Interference Contrast Microscopy. Int. J. Pharm. (158): 39-46.

H. Liu, P. Wang, X. Zhang, F. Shen, C.G. Gogos (2010). Effects of Extrusion Process Parameters on the Dissolution Behavior of Indomethacin in Eudragit® E PO Solid Dispersions. Int. J. Pharm. (383): 161-169.

H. Liu (2010). Hot Melt Mixing/Extrusion and Dissolution of Drug (Indomethacin) in Arylic Copolymer Matrices. PhD Dissertation, New Jersey Institute of Technology, Newark, NJ.

P. Wang, L. Zhu, S. Teng, Q. Zhang, M.W. Young, C.G. Gogos (2009). A Novel Process for Simultaneous Milling and Coating of Particulates. Powder Technol. (193): 65-68.

P.J. Marsac, T. Li, L.S. Taylor (2008). Estimation of Drug–Polymer Miscibility and Solubility in Amorphous Solid Dispersions Using Experimentally Determined Interaction Parameters. Pharm. Res 26(1): 139-151.

R. Supabphol, P.J. Stewart (1996). Aggregation during the Dissolution of Diazepam in Interactive and Granulated Mixtures. Pharm. Sci. (2): 233-236.

R.J. Chokshi, H.K. Sandhu, R.M. Iyer, N.H. Shah, A.W. Malick, H. Zia (2005). Characterization of Physico-mechanical Properties of Indomethacin and Polymers to Assess their Suitability for Hot-melt Extrusion Process as a Means to Manufacture Solid Sispersion/Solution. J. Pharm. Sci.(94): 2463-2474.

S. Qi, A. Gryczke, P. Belton, D.Q.M. Craig (2008). Characterization of Solid Dispersions of Paracetamol and Eudragit® E Prepared by Hot-melt extrusion using Thermal, Microthermal and Spectroscopic Analysis. Int. J. Pharm. (354): 158-167.

S. Teng, P. Wang, L. Zhu, M.W. Young, C.G. Gogos (2009). Experiemntal and Numerical Analysis of a Lab-scale Fluid Energy Mill. Powder Technol. (195): 31-39.

S.U. Yoo, S.L. Krill, Z. Wang, C. Telang (2009). Miscibility/Stability Considerations in Binary Solid Dispersion Systems Composed of Functional Excipients towards the Design of Multi-component Amorphous Systems. J. Pharm. Sci. (98): 4711-4723.

W. Doll, L. Konczol, L. Bevan (1985). in: H.F. Mark, N. Bikales, C.G. Overberger, G. Menges, J.I. Kroschwitz (Ed.), Encyclopedia of Polymer Science and Engineering, 2nd ed. Wiley-Interscience, New York, NY. 9: 745-760.

Z.Tadmor and C.G. Gogos (2006). Principles of Polymer Processing, 2nd Edition ed. John Wiley & Sons, Inc.